An Experimental Investigation of JP-7 and *n*-Heptane Extinction Limits in an Opposed Jet Burner

by

Janet L. Convery

Thesis submitted to the Faculty of Virginia Polytechnic Institute and State University in partial fulfillment of the requirements for the degree of

Master of Science

in

Mechanical Engineering

Approved:

_____

W. F. O'Brien, Committee Chair

_____ _____

G. L. Pellett U. Vandsburger

October 27, 2005

Blacksburg, VA

Keywords: JP-7, heptane, opposed jet, counterflow diffusion flame, extinction limit

An Experimental Investigation of JP-7 and *n*-Heptane Extinction Limits in an Opposed Jet Burner

by

Janet L. Convery

(ABSTRACT)

Propulsion engine combustor design and analysis require experimentally verified data on the chemical kinetics of limiting fuel combustion rates. Among the important data is the combustion extinction limit as measured by the maximum global strain rate on a laminar, counterflow, non-premixed flame. The extinction limit relates to the ability to maintain combustor operation, and the extinction limit data for pure fuel versus air systems provide a relative reactivity scale for use in the design of flame holders.

Extinction limit data were obtained for nine fuels by means of a laminar flame experiment using an opposed jet burner (OJB). The OJB consists of two axi-symmetric tubes (for fuel and oxidizer separately), which produce a flat, disk-like, counterflow diffusion flame. This paper presents results of experiments conducted in an OJB that measured extinction limits at one atmosphere for vaporized *n*-heptane, the Air Force-developed fuels JP-7, and JP-10, as well as methane, ethane, ethylene, propane, butane, and hydrogen.

In hypersonic aircraft development it is desirable to design a Scramjet engine that is operated on hydrocarbon fuel, particularly JP-7 due to its distinct properties. This study provides key data for JP-7, for which very limited information previously existed. The interest in *n*-heptane is twofold. First, it has undergone a significant amount of previous flame structure and extinction limit study. Second, *n*-heptane (C_7H_{16}) is a pure substance, and therefore does not vary in composition, as does JP-7, which is a variable mixture of several different hydrocarbons. These two facts allow a baseline to be established by comparing the new OJB results to those previously taken. Additionally, the existing data for *n*-heptane, for mixtures up to 26 mole percent in nitrogen, is extended to 100% *n*-heptane, reaching an asymptotic limit. Extinction limit data for the

two fuels are given with a comparison to hydrogen and several other gaseous hydrocarbon fuels. Complete experimental results are included.

ACKNOWLEDGEMENTS

First and foremost, I would like to thank my advisors, Dr. Walter O'Brien from Virginia Tech and Dr. Gerald Pellett from NASA Langley Research Center. Their guidance and seemingly endless knowledge has been a greater help than I can express. Both have not only been academic mentors, but have also kept my best interests in mind in my career and life since the start of my Master's program.

I thank my parents, James and Aimee Convery, for always believing in me, for their love and support, and not least of all for their financial support. I thank my father for teaching me integrity, humility, dedication, and how to lead. I thank my mother for teaching me compassion, generosity, and well roundedness, and for her prayers.

I give many thanks to all of my family, particularly my siblings, Mary, Rich, and Kathy, and to all of my friends for showing me love, support, and countless great times. I would never have finished this program without them. Also, I would not have gained nearly as much from the NIA graduate program if it hadn't been for my fellow graduate students. I especially thank my sister, Mary, whose footsteps have led me this far.

Finally, I'd like to acknowledge NASA Langley Research Center for funding this research and providing me with an excellent mentor, Jerry Pellett, and for the great group of people in the Hypersonic Air Breathing Propulsion Branch. I'd also like to thank the National Institute of Aerospace, who arranged and supported the fellowship program between NASA and six outstanding universities, and where I took classes and met all of my fellow graduate student friends.

TABLE OF CONTENTS

LIST OF FIGURES

LIST OF TABLES

LIST OF SYMBOLS

Roman Symbols

a	global axial strain rate
a_{300K}	global axial strain rate at 300 Kelvin
$a_{300K1atm}$	global axial strain rate at 300 Kelvin and 1 atmosphere
A	frequency factor
D	diameter
D_1	first Damköeler number
D_n	nozzle diameter
D_t	tube diameter
k_T	chemical kinetic rate coefficient
l	reactor length across flame
L	tube separation distance
$\dot{m}$	mass flow rate
MW	molecular weight
n	number of moles
p	pressure
p_r	ambient (room) pressure
$\dot{R}$	reaction rate
R_u	Universal gas constant
t_R	reaction time
T	temperature
T_r	ambient (room) temperature
U	velocity
U_{air}	cross-section average air side velocity at tube/nozzle exit
U_{fuel}	cross-section average fuel side velocity at tube/nozzle exit
V	volume
$\dot{V}$	volumetric flow rate
z	compressibility factor for non-ideal gas

Greek Symbols

Δ	change in quantity
μ	dynamic viscosity
n	normal/straight chain
ρ	density
τ_c	characteristic chemical time
τ_f	characteristic flow time

Subscripts

1atm	at 1 atmosphere
300K	at 300 degrees Kelvin
air	air side
c	chemical reaction time
f	flow time
fuel	fuel side
o	standard state
r	room
R	reaction
T	rate coefficient as a function of temperature

Abbreviations

CH_4	methane
C_2H_4	ethylene
C_2H_6	ethane
C_3H_8	propane
C_4H_{10}	butane
C_7H_{16}	heptane
CFDF	counterflow diffusion flame
JP	jet propellant
LDA	laser Doppler anemometry
N_2	nitrogen
NASA	National Aeronautics and Space Administration
OJB	opposed jet burner

PIV	particle imaging velocimetry
SLPM	standard liters per minute at 0˚C, 1 atm
TC	thermocouple
w/	with

Units of Measurement

atm	atmospheres
˚C	degrees Celsius
g	grams
K	Kelvin
kPa	kilopascals
L	liters
mm Hg	millimeters of mercury
mm	millimeters
mol	moles
psia	pounds per square inch atmospheric
psig	pounds per square inch gage
s	seconds

Chapter 1

INTRODUCTION

1.1 Laminar Diffusion Flame Characterization

Understanding non-premixed, turbulent combustion has been important for air breathing engine applications since their conception. However, combustion in a turbulent environment is so complex that it is very difficult to model and understand. Therefore, to simplify the problem, it is often necessary to perform laminar flame studies. In some instances it is appropriate to model turbulent flames in a combustor as an ensemble of many stretched and distorted laminar flamelets [1-4]. In other cases, this may not be possible [5], however laminar flame studies are still very valuable as they provide a relative reactivity scale for various fuels.

For the combustion application of gas turbine, ramjet, and Scramjet engines, fuel and air are not premixed prior to ignition in the combustion chamber, causing non-premixed/diffusion flames to form. This presents the need to understand how different fuels will behave in this environment. By studying laminar diffusion flames in which experimental data are unaffected by turbulent mixing, and can be analyzed more exactly and are more likely reproducible, fuels can more easily be characterized and compared to one another.

Among the important combustion data used to classify fuels is the extinction limit for a standard fuel, as it pertains to the ability to hold or maintain a flame in an engine or combustion chamber. It is of great interest to develop a reactivity scale of extinction limits for hydrogen and hydrocarbon fuels to aid in both fuel selection for an engine, and in combustion chamber design. The opposed jet burner (OJB), which produces a counterflow diffusion flame (CFDF) structure, was pioneered by Potter [6,7], and has been widely used to examine flame characteristics for over five decades. This device is ideal for determining extinction limits of a given fuel in a particular environment because of the wide, flat flame it produces. The flat flame becomes thinner and thinner as flow rates are increased and extinction is neared, such that it can be approximated as one dimensional, allowing for the use of simplified 1-D Navier-Stokes equations. Because of its simplicity and effectiveness, the OJB approach was employed in this research.

The OJBs used in this study consist of two axi-symmetric, opposing tubes (or tapered nozzles), from which oxidizer (air) and fuel flow separately to form a stagnation plane between the two fluid streams. At this interface an ignition source is introduced to produce a non-premixed, flat, disk-like flame. The extinction limit of this CFDF is found by slowly increasing the mass flow rates of the fuel and air while keeping the flame centered between the two tubes, until the flame extinguishes. At blowoff, the flame may be extinguished all together, or in most cases may only blow out in the center, producing a ring-shaped flame. In the latter case, the flame may be restored to its original form of a disk if the flow rates are reduced, providing further information about the nature of the fuel.

1.2 Fuel Applications

With recent advances in hypersonic aircraft utilizing Scramjet (super-sonic combustion ramjet) engines, a hydrocarbon-fueled combustor is very attractive to programs of the National Aeronautics and Space Administration (NASA) and the U.S. Air Force and Navy. In March 2004 NASA's X-43A hypersonic aircraft reached a world record speed of Mach 6.8 for an aircraft powered by an air-breathing, Scramjet engine, and in November of that year the X-43A reached Mach 9.6, again setting a new world record. This aircraft, pictured in Figure 1.1, was fueled by hydrogen. NASA and the U.S. military would now like to develop a hydrocarbon fueled Scramjet for several reasons including: simplicity of fuel handling and storage, high fuel energy density, and cost savings [8]. NASA's X-43C model aircraft was designed to use the Air Force jet propellant, JP-7, combined with an undetermined "cold start" system, in its Scramjet engine. JP-7 is a mixture of several hydrocarbons that falls into the fuel category of kerosene. The X-43C program's future is uncertain at this time, however it is still greatly desired to gain a better understanding and classification of JP-7 fuel.

Because JP-7 is a mixture of hydrocarbons and can vary from batch to batch, *n*-heptane, a pure fuel, was chosen to establish a standard database for the experimental apparatus and ensure repeatability of data. Extinction limits have been determined in previous studies for relatively small percentages of *n*-heptane (up to 26 mole %) mixed with nitrogen diluent. The resulting data were used for a baseline of comparison for data

taken with the current system. Also, larger percentages of *n*-heptane in nitrogen were tested all the way up to pure fuel. This provides new data for a fuel that has been widely used to evaluate combustion systems.

NASA Dryden Flight Research Center Photo Collection
http://www.dfrc.nasa.gov/gallery/photo/index.html
NASA Photo: ED99-45243-01 Date: 1999 Photo by: NASA

X-43A Hypersonic Experimental Vehicle - Artist Concept in Flight

Figure 1.1. Artist's concept of NASA's X-43A hypersonic aircraft [9].

1.3 JP-7 and *n*-Heptane Experimental Research

The primary goal of this research was to obtain experimental extinction limit data for *n*-heptane (C_7H_{16}) and JP-7 fuels burning in atmospheric air. The intermediate goal was to gain a better understanding of this OJB system and how it relates to other diffusion flame burners. Both of these goals were attained successfully.

The following section of this paper presents the results of an extensive literature search, providing the necessary background information to understand the need and approach taken for this experimental work. Chapter 3, The Investigation, provides a detailed layout of the specific goals of the research. It is followed by the Method of Analysis, which explains how the experimental data was analyzed, and the Plan of Experiment, which describes how the data were obtained. Chapter 6 presents the results with discussion, followed by conclusions in the final chapter.

Chapter 2

BACKGROUND/LITERATURE REVIEW

This chapter provides a review of the underlying concepts critical to the experimental investigation. First the nature of diffusion flames will be described, including a history of previous study methods. Next the importance of doing a laminar diffusion flame experiment as opposed to a turbulent flame study is discussed. A section on flame extinction limits and their importance in classifying fuels for the purpose of combustor design follows. (The methodology and equations for determining extinction limits in this investigation is presented later in Chapter 4.) The fourth section of this chapter describes the opposed jet burner (OJB) in detail; it is the apparatus chosen to study extinction limits of laminar diffusion flames in this research. The final two sections give details of *n*-heptane and JP-7 and the justification for their selection as the fuels chosen for study.

2.1 Diffusion Flames

A diffusion flame occurs when fuel and oxidizer meet in the region of combustion without prior mixing, where fuel molecules diffuse towards the flame from one direction and oxidizer molecules diffuse towards the flame from the opposite direction [10]. Burke and Schumann first studied these non-premixed/diffusion flames in detail in the late 1920s, recognizing both a lack of previous study and a vast area of application, such as oil furnaces and rocket engines [7,11]. They performed jet diffusion flame experiments using concentric tubes with fuel flowing upward from the inner tube and oxidizer flowing around it from the outer tube, where combustion was confined to a surface they called the "flame front." At this interface the flame was thin enough that it was considered a geometrical surface, allowing for simplified numerical predictions to be successfully compared to experimental results [7]. This classic flame sheet theory requires an infinitely fast chemical reaction; an assumption that cannot apply to a highly strained flame near or at extinction, where aerodynamic and diffusion times are decreased [2]. Nevertheless, their groundbreaking research paved the way for future diffusion flame study.

Several types of burners were later developed for the study of diffusion flames, four of which are shown in Figure 2.1 [12]. The Type I burner (as denoted by Tsuji), which will be referred to as the opposed jet burner (OJB), was first used experimentally by Potter and Butler [6], following separate theoretical studies by Zeldovitch [13] and Spalding [14], which showed that an increase in fuel and oxidant flow would cause extinguishment of a diffusion flame. The Type I burner consists of two opposing, axis-symmetric tubes, one for fuel and one for oxidant. A disk-shaped flame forms near the stagnation plane of the opposing fluid jets. The flame produced by the OJB is very flat, and at extinction is nearly one-dimensional, allowing for a simplified analysis. The OJB is employed in this experimental research, and will be discussed at length throughout the paper. It is a relatively simple device that is well suited to study extinction limits, flame strength and flame structure [1,5,6,12,15-22].

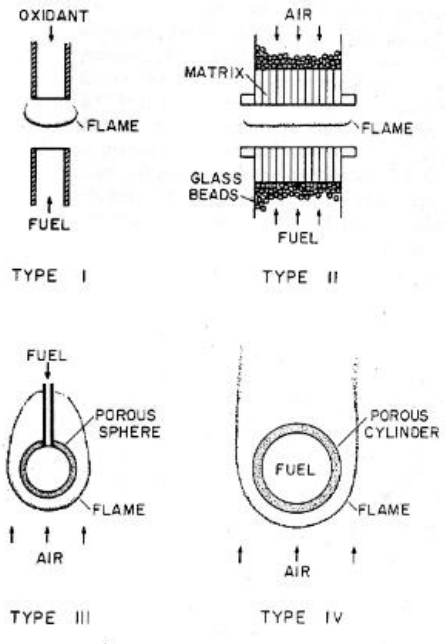

Figure 2.1. Four types of diffusion flame burners [12].

The Type II burner is similar to the OJB with fuel and oxidizer flowing from opposite sides, in this case flowing through an enlarged, uniform matrix instead of through smaller single tubes or nozzles. The matrix of beads causes disruptions in the fluid path, randomizing the flow velocity distributions. It is experimentally more

complex than the Type I burner; it typically requires much higher fuel flow rates, and cooling requirements often constrain the range of allowable fuel concentration. It was first studied by Pandya and Weinberg, and is particularly useful in the study of flame structure in the presence of an electric field [12,23].

The final two diffusion flame burner types include a porous sphere and a porous cylinder respectively, through which fuel flows as oxidizer flows around it. The Type III burner was employed in early studies by Spalding [14], and the Type IV burner was used extensively by Tsuji and Yamaoka and others [24-27]. The two-dimensional nature of these flames makes them inherently more complex than the axi-symmetric OJB flames. Both types are suitable for studying extinction limits and flame strength. The Type IV burner is also used in studying flame structure characteristics, but is not suited for examining effects of an electric field [12].

2.2 Laminar Flames

Two important questions that must be addressed in this research are: why is a laminar flame study desirable and how does it correlate with a turbulent application? The answer to the first question is relatively simple. Laminar flames are much less complex and are easier to understand and model than the turbulent flames seen in an engine combustor, and most other practical applications. In the experiments performed in this research, repeatability was critical, and could be more readily obtained by a laminar flame study. Also, exact numerical modeling is only possible with laminar flames, which allows for analytical results and accurate simulations to be compared to experimental data [20].

The second question is more complex. The turbulent diffusion flames seen in an engine combustor contain vortices in areas of recirculation as pictured in Figure 2.2 [2]. Within these vortices, the turbulent flame sheets may consist of ensembles of many stretched and distorted laminar diffusion flamelets, in which laminar flamelet modeling can be applied [1-4]. In these cases and in others where laminar flamelet theory is not appropriate, a great deal of knowledge can be gained by understanding the characteristics of laminar diffusion flames, particularly their extinction and restoration limits, as discussed in detail in the following section.

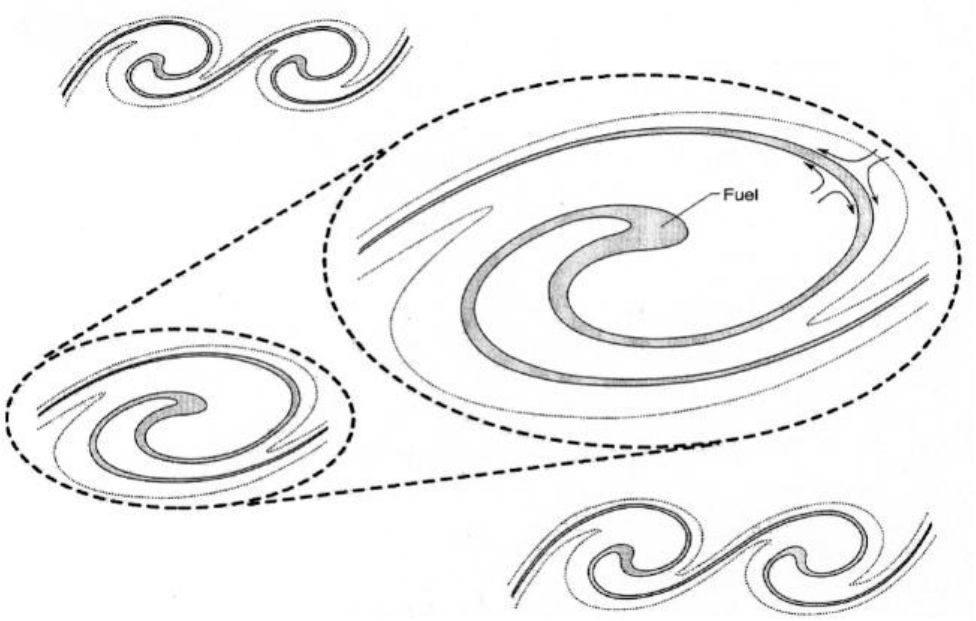

Figure 2.2. Turbulent flames composed of laminar flamelets [2].

2.3 Extinction Limits

The concept that diffusion flames would become extinct at a specific point as flow rates of fuel and oxidizer were increased was first proposed by Zeldovich [13] and Spalding [14], and tested experimentally by Potter and Butler, later with Heimel, [6,7] beginning in the early 1950s. Their research demonstrated that there is a limit in fuel and oxidizer flow rate at which the chemical reaction is not fast enough to keep up with the rate of diffusion, and the flame goes out. Potter, *et al*, referred to this point as a "breaking" of the flame because the flame appeared to break apart at the center where flow rates were highest; this phenomenon was later referred to as blowoff or extinction [1,6,16-22,28]. The concept of extinction is explained clearly by the parameter known as the first Damköeler number, D_1, defined as the ratio of characteristic flow time to characteristic chemical reaction time [10,12,28-31]:

$$D_1 \equiv \frac{\tau_f}{\tau_c} \tag{2.1}$$

When the chemical reaction time is much shorter than the diffusion/flow time, $D_1 >> 1$, and there is a fast, intense chemical reaction. Conversely, when the chemical reaction time is much longer than the flow time, $D_1 << 1$, and the chemical reaction is slow because

the reactants do not release the energy stored in their chemical bonds [30]. For a non-reacting flow, D_1 is zero, and for an equilibrium flow, it is infinite [28]. It is an infinite D_1 that is implied in the assumptions of the classic Burke-Schumann flame in which the diffusion flame is a flame sheet. Fendell reports that it is a sudden transition between branches of intermediate Damköeler numbers that accounts for the phenomena of both ignition and extinction of a flame [30]. Extinction is reached at a low Damköeler number (typically near one) when the fuel and oxidizer are no longer in contact long enough for the chemical reaction of combustion to take place [10,12,28-31].

In the case of the OJB (Type I) and Type II flames pictured in Figure 2.1, extinction of the disk-shaped flame typically occurs at the center of the flame where the radial strain rate tends to be the highest, and a ring-shaped flame remains [1]. For the Type III and IV burners, extinction occurs when the flame blows off from the forward stagnation region into a "wake" flame [12]. The key parameter of interest that can readily be measured at extinction is the global axial input strain rate at the airside edge of the stretched flame. The method for calculating strain rate will be demonstrated in Chapter 4. Compiling extinction limits for many fuels is of great interest in order to create a reactivity scale in which the fuels can be compared relative to each other.

2.4 The Opposed Jet Burner

Of the four types of counter-flow diffusion burners mentioned, the OJB was chosen for reasons including its experimental simplicity, its effectiveness in determining reproducible extinction limits, and the extensive experience and knowledge of fellow researchers with its operation [1,16-22]. This section describes the flow field of an OJB, and the use of nozzles versus tubes and their respective input flow profiles.

2.4.1 Flow Field

As shown in Figure 2.1, the Type I OJB consists of fuel and oxidant flowing towards each other from opposing tubes (or tapered nozzles). For cold flows in which the flame has not yet been ignited, the axial velocity of each jet decreases linearly until it reaches stagnation within the zone of impingement. At the stagnation point (surface) some diffusional mixing occurs where zero axial velocity is reached, and the fluid elements are accelerated radially outward. When a flame is present, however, the flow

fields are altered and the axial velocity no longer decreases linearly in the vicinity of the flame where heat from the flame causes acceleration in the flow. The predicted axial velocity profile was first developed by Hahn and Wendt, and is shown in Figure 2.3 (modified by Guerra, *et al*) [28,32]. As the figure demonstrates, the axial velocity decreases linearly from the tube exit as in the cold flow case, until the flame zone is reached. Two virtual stagnation points, different from both the actual and the cold flow stagnation points, exist for the jets. The linear axial input velocity gradient on the airside edge is critical in analysis because it is typically used to determine the imposed strain rate on the flame, which is the key parameter of interest at extinction.

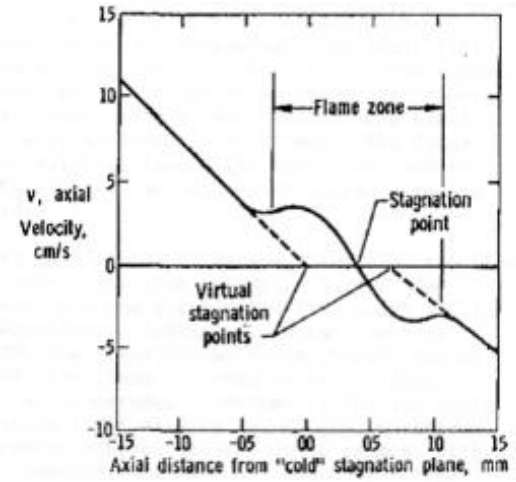

Figure 2.3. Predicted axial velocity profile for a 3.6 1/s flame stretch rate [28,32].

In addition to altering the velocity field, diffusion and combustion of highly reactive, low molecular weight species typically cause the flame to be located on the airside of the stagnation plane between the fluid streams, as pictured in Figures 2.4 [1,2]. This phenomenon was predicted by Spalding, at least for the case of pure fuels, and later demonstrated by Potter, *et al*, for hydrogen and several hydrocarbons [7,33]. The latter study involved the introduction of magnesia powder in to the air and fuel streams in separate experiments. When added to the air jet, the magnesia particles were seen glowing as they passed through the flame, whereas for addition to the fuel flow, the particles did not enter the flame [7]. Later experiments have shown the same results as in Figure 4.2 using more advanced techniques including laser Doppler anemometry (LDA),

particle imaging velocimetry (PIV), and focusing schlieren [19,20,34]. The flame is located where the mixture fraction is nominally stoichiometric [10]. Therefore, the amount that the flame deviates from the stagnation plane depends on the fuel used; for example the hydrogen flame sits much farther on the oxidizer side than flames for other hydrocarbons, the reason being that it diffuses much faster and farther into the oxidizer stream [1]. For some heavy hydrocarbons, the flame may reside slightly on the fuel side in a case where oxidizer diffuses more into the fuel stream before reaction occurs [35].

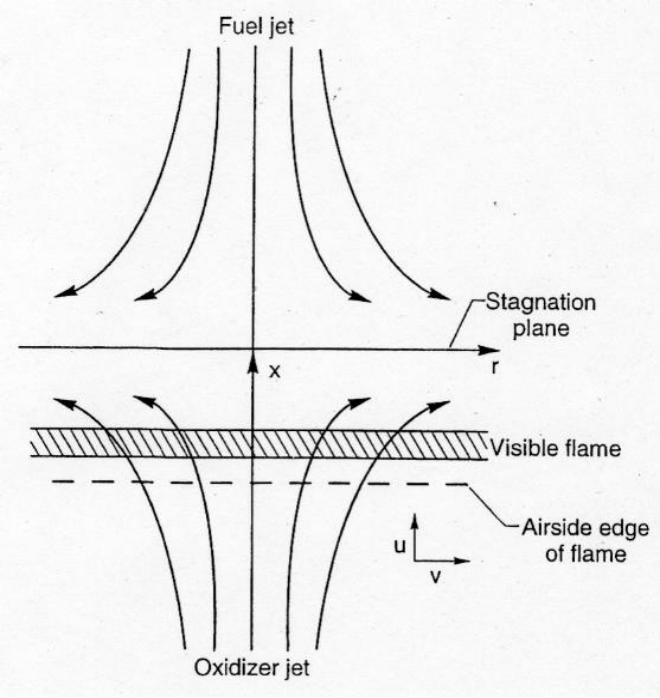

Figure 2.4. Flame and stagnation plane locations for opposed jet combustion [1].

As a result of the fuel diffusing into the oxidizer side of the stagnation plane, it has been observed in this experiment and in previous work that the residual ring-shaped flame "jumps" slightly towards the fuel tube at the moment that extinction is reached [1,16,28]. This is because the flame blows out in the center, and therefore the absence of central heat release shifts axial flow to the stagnation plane. Likewise, when the flame is restored as flow rates are decreased and a flame forms again in the center of the disk, the flame shifts slightly back towards the oxidizer side as fuel diffuses into the oxidizer jet [2].

2.4.2 Nozzle versus Tube

The principal difference between convergent nozzle and straight tube OJBs is the axial input velocity profile of fuel and oxidizer (in this case air) at the respective exit areas. For a tube OJB, tube lengths are chosen such that fully developed flow is established, producing a two-dimensional parabolic flow profile in the air and fuel jets. For a nozzle OJB, the fuel and air exits are shaped such that an ideally one-dimensional plug flow profile is approximated, yielding a flat, uniform impingement flow. The benefit of the nozzle plug flow profile is that it allows for a simplified one-dimensional analysis, based on achievable plug flow inputs, for calculating the axial strain rate at extinction (equal to the axial input velocity gradient). Thus it appears more suitable for 1-D numerical modeling. The first detailed 1-D model was developed for idealized potential flow inputs for boundary layer flows; later an eigenvalue solution was developed for the plug flow boundary conditions and both 1-D solutions are based on Navier-Stokes stream functions for boundary layer flows [3]. The 1-D plug flow profile solution requires large jets (ideally infinite), and is therefore best suited for large diameter nozzle or matrix-filled tube jets with a small jet separation (less than 1 diameter), minimizing boundary layer effects.

For pure fuels, the strain rate at extinction, proportional to the air velocity divided by the effective (overall) diameter (U_{air}/D), is quite high, while the effective Reynolds number varies with jet velocity multiplied by diameter (UD). This dual condition imposes the limitation that jet diameter must remain small enough to achieve extinction and maintain laminar flow.

Finally, the result of impinging nozzle flows is a somewhat non-ideal flow profile, sometimes referred to as a "top hat" shape, which is also more sensitive to nozzle separation, leading to data with poorer reproducibility than the tube OJB [1,6,7,20]. The flame that results from Rolon's observed non-ideality in the plug flow profile for a nozzle OJB deviates noticeably from an otherwise flat disk flame. The central region of the flame is about 5 to 10% thicker than the flat outer portion [18-22,36], which reflects decreased axial input velocities in the central region.

Thus because the nozzle OJB is less than ideal, based on a combination of reasons, the tube OJB system was chosen for this experiment. The tube parabolic flow profile differs markedly from the nozzle plug flow profile such that small tubes with a large (needed) separation (1.5 to 3 diameters) do not adversely affect the flow profile and resultant extinction limits. The flow remains very nearly parabolic as it flows out of the tubes, which allows for experimental simplicity and guaranteed boundary conditions. Another objective in using a tube OJB in this experiment was to compare tube OJB extinction limit data to previously taken nozzle OJB data to better understand the relationship between the two. This relationship is discussed in detail in the Method of Analysis.

2.5 *n*-Heptane Fuel

Normal or straight-chain heptane fuel (written *n*-heptane) has the chemical formula C_7H_{16}, and is of the alkanes/paraffins family classification of fuels, such that it is single-bonded only [10]. The testing of *n*-heptane is valuable for several reasons. It is a pure fuel; this means that its composition is fixed and will not change during the vaporization process, unlike JP-7, which is a variable mixture of several hydrocarbon fuels. Therefore, *n*-heptane's experimental repeatability is excellent, whereas different batches of JP-7 may yield slightly different results. It serves well as a surrogate fuel for other hydrocarbon mixtures because of its relative simplicity, and it has been referred to in defining octane number [37]. More importantly, it has been studied extensively in the past and is well defined for both flame structure and extinction limits [31,37-39]. All of these facts make *n*-heptane an ideal choice for defining a baseline for the liquid fuel experimental test configuration. In addition, past extinction limit studies have been limited to mixtures of about 26 mole percent of *n*-heptane in nitrogen [38], so it is also of great interest to complete the data set between 26% and pure fuel.

2.6 JP-7 Fuel

The jet-propellant fuel JP-7 is an Air Force-developed fuel that continues to be important in the area of hypersonics. Because of its distinct properties such as its endothermic nature, thermal stability, good ignition at high temperature, and high flash

point, it was developed for use in supersonic aircraft such as the SR-71 Blackbird [40,41], and it is currently the hydrocarbon fuel of choice for use in Scramjet engines.

JP-7 and other aviation fuels consist primarily of hydrocarbons compounds such as paraffins, cycloparaffins, aromatics, and olefins; paraffins and cycloparaffins being the major components [40,42-44]. Paraffins have a high heat release to weight ratio (high energy density) and burn cleaner than many other hydrocarbons. Cycloparaffins increase fuel density and provide a lower freezing point for the fuel. Aromatics are a better source of energy than some hydrocarbons, but are limited in the fuel mixture due to sooting [40]. An approximate formula for JP-7 determined from estimated molecular weight and average composition is $C_{12}H_{25}$. The composition of JP-7 varies from batch to batch due to varying refinery conditions, crude oil sources, and season of production, and can change for a given batch as the fuel ages [45]. It falls into the general category of fuels called "kerosene," along with many other jet-propellant fuels [41].

Chapter 3

THE INVESTIGATION

The primary goal of this research is to determine non-premixed extinction limits for vaporized *n*-heptane and JP-7 fuels burning with atmospheric air. In order to obtain these results, several other steps were first made in order to verify certain critical factors of the experimental test setup. This chapter will describe each of the tests performed to establish the opposed jet burner (OJB) system, and how they pertain to the overall goals of the research. These experiments include a comparison of the current test data to previous OJB test data and numerical analysis, a comparison of data from the gaseous fuel test configuration to the liquid fuel test configuration, an evaluation of different tube sizes in the OJB, and finally a comparison of nozzle OJB to tube OJB data. The results of the experiments described here will be presented in Chapter 6.

3.1 Hydrogen Study

The first experiment was performed using pure hydrogen fuel. Extinction limits were taken using a 2.9 mm inner diameter tube OJB for comparison with previous experimental data from a similar OJB, and for comparison with numerical analysis. The previous experimental setup utilized a 2.7 mm tube. The numerical analysis was performed using a two-dimensional parabolic inflow boundary condition, which models the 2-D flow profile of a tube OJB [2]. This evaluation with hydrogen was important because it established a baseline for the current gaseous fuel system.

3.2 Propane Study

Next, the liquid fuel vaporization setup was verified against the gaseous fuel setup in an experiment using pure propane fuel. The propane was heated in the same exact process as the liquid fuels in a closed system and tested using the same system temperatures and pressures. This provided a direct comparison of the gaseous and liquid configurations. Then fresh propane was tested again in the heated, liquid fuel setup in an open system where fuel flowed through the system from a fuel tank. This second test of the liquid vaporizer system examined whether or not the lengthy (about two hour) heating process altered the fuel and resulting data, and it provided a measure of the small effect

of heated fuel input on extinction limits. Both of these test results were compared to results from the original gaseous fuel configuration, providing necessary checks to support the validity of the liquid fuel system.

3.3 Tube Size Comparison

The purpose of this experiment was to examine the effect that tube size has on the extinction limit. Therefore, four tubes of varying diameter were tested using the following gaseous hydrocarbons: methane, ethane, propane, and ethylene. The nominal inside tube diameters used were 2.9 mm, 5.0 mm, 7.5 mm, and 9.3 mm. The diameter of the tube is a critical parameter in extinction limit experiments because the calculated strain rate at extinction depends inversely on diameter cubed.

3.4 Tube to Nozzle Comparison

The final experiment prior to testing *n*-heptane and JP-7 was to compare data from the current tube OJB to data previously taken with a well-characterized nozzle OJB [16,17]. The two test configurations have different input flow profiles and therefore different equations for determining strain rate at extinction. Consequently, it is necessary to clarify the difference in resulting data. Methane, ethane, propane, and ethylene were used again to make this comparison.

3.5 JP-7 and *n*-Heptane

Finally, using the knowledge gained from these four validation experiments, vaporized *n*-heptane and JP-7 were tested, and the data were analyzed. This was the chief objective of the research: to determine extinction limits of *n*-heptane and JP-7 fuels, both pure and in mixtures with nitrogen diluent.

Chapter 4

METHOD OF ANALYSIS

This chapter presents the methodology used to determine extinction limits for a given fuel using an opposed jet burner (OJB). First, a physical description of pre-extinction and post-extinction flames is presented. This is followed by the approach and equations used to calculate the global strain rate on a flame at extinction, which is the parameter of interest in this experiment.

4.1 Flame Extinction

A schematic of the OJB in a combustion box is shown in Figure 4.1. There are three different tube sizes pictured, but only one set is used at a time. The varying tube sizes used in this research will be discussed in detail in the Results and Discussion chapter. The main purpose of presenting Figure 4.1 is to show the free-floating flame centered between the axis-symmetric air and fuel tubes. The flame takes on the shape of a disk initially, and is maintained in the center of the tubes as flow rates are increased using metering valves. The disk flame that is present before extinction is pictured in Figure 4.2, taken from a previous OJB test setup. As the input flow rates are increased the flame is stretched radially outward, increasing the strain on the flame. The local input axial strain rate and resultant radial strain rate tend to be highest at the center. The overall increase in strain rate causes the flame to become thinner and more nearly one-dimensional. Previous detailed studies have shown the effective thickness of both nozzle and tube OJB flames vary as the square root of applied strain rate [1,20], which is considered classical behavior of a CFDF. At extinction, the strain rate in the center is too high to maintain a flame, and the flame breaks and blows off into a ring-shaped flame as pictured in Figure 4.3, or occasionally the flame blows off all together. Extinction occurs suddenly at the temperature point where enthalpy release can no longer keep up with the heat loss from the strained flame [22]. When a ring flame is formed, the flow rates can be reduced until the flame restores or relights in the center, forming a disk flame again.

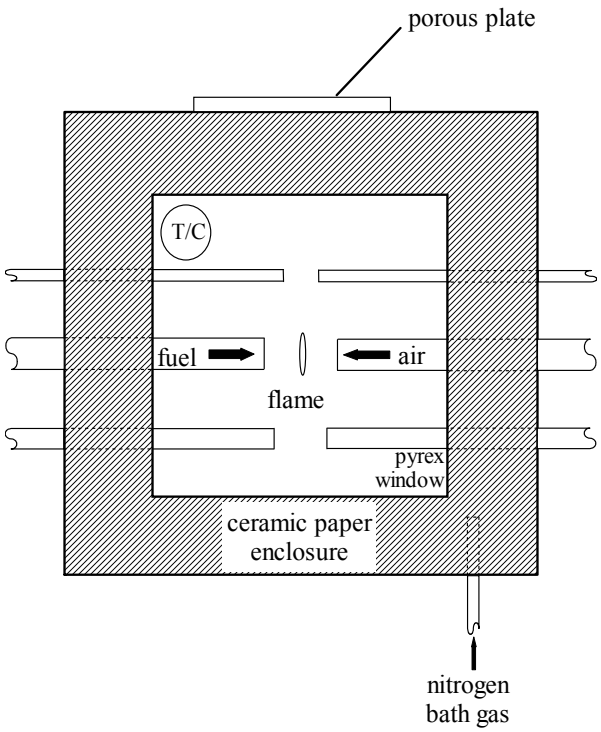

Figure 4.1. Triple tube opposed jet burner contained in the combustion box.

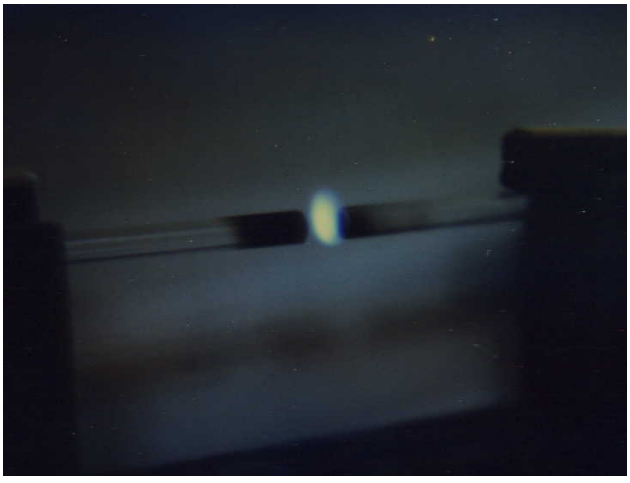

Figure 4.2. Disk-shaped counterflow diffusion flame before extinction.

Figure 4.3. Ring-shaped counterflow diffusion flame after extinction.

The tubes are spaced between one and a half and three tube diameters apart. It has been demonstrated that varying the tube gap in this range has a negligible effect on the resulting extinction data [1,22]. Also, it is important that the tubes are spaced far enough apart to prevent flame anchoring and ensure a free-floating flame, despite minor, unavoidable flow variations [1,20,22].

The OJB tube configuration was horizontal for this experiment, as pictured above. Previous OJB systems have used both horizontal and vertical setups, and in the latter case, experiments have been performed with air coming from the top tube/nozzle and fuel from the bottom, and vice versa. In all three configurations the effect of buoyancy was negligible such that the resulting data were nearly identical [1,20].

As Chapter Two explains, the extinction limit for a fuel occurs at the flow rates at which the fuel and air are in contact for a shorter period of time than is required for the chemical reaction of combustion to take place adequately [10,12,28-31]. At the moment of extinction the standard volumetric flow rates of air, and if available, fuel, were recorded in standard liters per minute (SLPM). (Fuel flow rates could not be measured via flow meter in the vaporized liquid fuel test configuration because the fuel stream was too hot and at such a low flow rate that there were no flowmeters that could operate under such conditions.) The velocity of the air flow was then calculated by dividing the

volumetric flow rate by the cross-sectional area of the tube, and was then used to determine strain rate as shown below.

4.2 Global Strain Rate Calculation

Strain rate of a flame (e.g. just before extinction) is generally measured from the centerline axial velocity gradient on the oxidizer side [1,3,5,12,20,22,36,38,46]. The axial velocity gradient becomes linear up to the flame front as shown in Figure 2.3, and as seen in previous experimental results [19,21,36,45,46]. Using an idealized plug flow profile described in Chapter 2, as in the case of a nozzle OJB, and recognizing that the flame is very nearly one-dimensional at the high strain rates near extinction, the axial velocity gradient at the airside edge is equal to twice the oxidizer (in this case air) velocity normalized by the nozzle diameter, having units of 1/s [1,3,12,16,20,29]:

$$a = 2\frac{U_{air}}{D_n} \tag{4.1}$$

In the case of a tube OJB, the flow is fully developed and therefore the profile is parabolic, also described in detail in Chapter 2. For a parabolic flow, the velocity at the centerline is twice the average velocity [47]. Since the flame blows out in the center where local strain rate is the highest (and flame breaking shuts down the supply of flame radicals), the recorded average velocity (taken from the volumetric flow rate) is only half of the velocity at the center of the flame where extinction occurs (i.e. U_{air} at the centerline = $2U_{air}$ measured) [34]. Therefore, it is expected that the strain rate for a tube would be proportional to that for a nozzle with the calculation requiring another factor of about two to take into account the velocity profiles. Experimental data have shown this factor to be closer to three in the case of hydrogen, and between two and three in the case of hydrocarbons [1,20]. The resulting experimental data in this study have yielded the following empirical relationship, which will be discussed in detail in Chapter 6:

$$a = 5.1\frac{U_{air}}{D_t} \tag{4.2}$$

The deviation from what was expected, which would be a strain rate of four times the air velocity normalized by tube diameter, is most likely due to the presence of flame and the flows deviating from ideal plug and parabolic profiles.

Another approach has been commonly used with the "Seshadri" matrix type burner, particularly by Seiser, *et al*, in previous experiments to determine *n*-heptane extinction limits using closely spaced (e.g. about 11 mm), large diameter (e.g. about 22 mm) matrix tube housings to approximate a plug flow profile [38]. Their setup varies from the above configuration in that the tube gap is less than half of one tube diameter, instead of greater than one and a half diameters. The key assumptions made in their analysis are that the Reynolds number is large, the mixing layer is a thin sheet at the stagnation plane, and the flow is rotational with plug flow boundary conditions. The expression derived to calculate strain rate, which is still defined as the axial velocity gradient on the oxidizer side of the flame, is as follows [5,31,37,38]:

$$a = \frac{2(-U_{air})}{L}\left[1 + \frac{U_{fuel}}{U_{air}}\sqrt{\frac{\rho_{fuel}}{\rho_{air}}}\right] \tag{4.3}$$

Later experiments using laser Doppler velocimetry (LDV) indicated that the mixing layer was in fact fairly thick and that the actual velocity gradient just ahead of the flame was about 40% smaller than that obtained using formula 4.3 [5]. Also, Rolon, *et al*, have pointed out that this calculated strain rate is inversely proportional to changes in tube spacing, and a much larger tube spacing (greater than 1.5 diameters) yields results much closer to actual measured velocity gradients [36]. The difference in the methodology used for the present research and that used in previous *n*-heptane research may account for the difference that will be shown in the data comparisons in Chapter 6.

4.3 Temperature and Pressure Corrections

After calculating global strain rate at extinction, the data were corrected for calculated reference temperature and room pressure to a preferred standard condition of 300 K and 101.325 kPa (1 atm). Because strain rate is calculated from the air velocity, the standard air temperature (273.15 K, used in mass flowmeter calibration) was always taken as the reference air temperature even when the fuel stream was heated in the case of vaporized liquid fuels. Past studies have calculated that air jet velocities at H_2-air extinction vary almost exactly linearly with input temperature from 300 K to 600 K [48]. Therefore, the applied temperature correction was estimated by multiplying by 300 K and dividing by the standard flowmeter calibration temperature:

$$a_{300K} = a\left(\frac{300}{273.15}\right) \tag{4.4}$$

The pressure correction is not nearly as straight forward. The derivation starts by recognizing that standard state volumetric flow rate can be written for any other p, T state as follows,

$$\dot{V}_o = \dot{V}\left(\frac{T_o}{T}\right)\left(\frac{p}{p_o}\right) \tag{4.5}$$

due to its dependence on temperature and pressure defined by the ideal gas law. Next, dividing both sides by the cross-sectional area yields:

$$U_o = U\left(\frac{T_o}{T}\right)\left(\frac{p}{p_o}\right) \tag{4.6}$$

For a plug flow profile, the reaction time based on reactor length, l, (across the flame) and average flow velocity is:

$$t_R = \frac{l}{U} \tag{4.7}$$

Recognizing that relative mole fractions of key reactants remain roughly proportional for this flow path, the corresponding molar concentrations must be directly proportional to pressure, and because the key reactions are bimolecular (two molecules reacting to form two different molecules) [10], the resultant reaction rate varies with pressure squared:

$$\dot{R} = k_T p^2 \tag{4.8}$$

Now small relative differences in temperature range in rate coefficient can be approximated as:

$$k_T \cong AT \tag{4.9}$$

such that

$$\dot{R} \cong ATp^2 \tag{4.10}$$

For comparative plug flow reactors with flame of length l, the number of moles reacted in each during combustion is thus estimated as:

$$\Delta n = \dot{R} t_R \cong ATp^2 \frac{l}{U} \tag{4.11}$$

Substituting for U yields:

$$\Delta n \cong \frac{AT_o}{p_o U_o} p^3 l \tag{4.12}$$

Here it is shown that the number of moles reacting in each case is estimated to depend on the pressure cubed. As a result, the pressure (and temperature) are corrected with the following equation:

$$a_{300K1tam} = a\left(\frac{300}{273.15}\right)\left(\frac{1}{p_r}\right)^3 \tag{4.13}$$

It should be noted that the pressure correction, despite being a factor of pressure ratio cubed, has a small effect on the data, and some previous studies have forgone a pressure correction [1].

Other experimental factors that did not affect extinction limits included temperature inside the combustion box, nitrogen purge rate, and combustion box ventilation. All of these parameters were monitored and deliberately varied to examine possible effects on the extinction data, and the effects were negligible.

4.4 Flame Strength

"Flame strength" is a common term used to describe counterflow diffusion flames, and has been defined differently by different experimenters. Potter, *et al*, first used the term "apparent flame strength" as the average mass flux of fuel and air jets at extinction [6,7]. Pellett, *et al*, later defined flame strength as air velocity at extinction, representing a maximum input velocity at which the flame can process air before it fails catastrophically due to heat loss and decreased reactivity [1]. For the purposes of this paper, the strength of a flame is recognized as being proportional to air velocity normalized by tube/nozzle diameter (U_{air}/D), adding a geometrical factor to the previous definition. Flame strength will therefore not be a calculated parameter, but rather a qualitative means of characterizing the flame holding potential of one fuel relative to another.

Chapter 5

PLAN OF EXPERIMENT

This chapter presents detailed test configurations of the opposed jet burner (OJB) as well as test procedures used to acquire experimental data. Experiments were performed using two test configurations, the first of which is referred to as the "gaseous fuel" setup where the fuel is in the gaseous state at standard conditions, and the second of which is referred to as the "liquid fuel" setup where the fuel is in the liquid state at standard conditions and must therefore be vaporized before entering the OJB. The fuels tested in the gaseous fuel setup included hydrogen, methane, ethane, ethylene, propane, and butane. The liquid fuels tested were *n*-heptane, JP-7, and JP-10. The gaseous fuel configuration is discussed first, followed by its operating procedure, and then the liquid fuel configuration is presented with its operating procedure.

5.1. Gaseous Fuel Test Configuration and Procedure

5.1.1 Gaseous Test Configuration

The gaseous fuel test setup is shown in Figure 5.1 including a key, which identifies the various valves, gages, etc. There were three different sized tubes contained in the combustion box labeled "opposed jet burner." One set of opposing tubes was used at a time. For the gaseous fuels the tube sizes were diameters of approximately 2.91 mm, 4.96 mm, 7.50 mm, and 9.25 mm (replacing the 7.5 mm tube in later experiments). The tube size was selected via the tube shutoff (16, 17, and 18) and selector (24) valves. The combustion box was made of a ceramic paper and held together loosely enough that if an explosion were to occur it would easily come apart for safety purposes. Also, the combustion box was ventilated at the top through a wire mesh such that exhaust gases were drawn up through the chemical fume hood (surrounding the entire setup). The bottom right of the drawing shows where the air entered the OJB system, starting at stem valve 19 and entering the box on the right through selector valve 24. The top right of the drawing shows the nitrogen supply for bath gas starting at stem valve 25. The bath gas was used to fill the combustion box and surround the OJB with an inert gas such that the oxygen only entered the system from the oxidizer tube (in this case as ambient air).

Various bath gases including nitrogen, helium, and argon have been shown in the past to have no effect on the resultant data when tube OJBs are used [1].

The left most part of the drawing shows the ventilated cabinet in which nitrogen and fuel tanks were kept for safety purposes. The system had the capability to flow nitrogen through the fuel lines via valve 8 to purge the system before and after an experimental run. During operation valve 8 remained closed, and nitrogen could be used as a diluent for the fuel if it were allowed to flow through the glass bead mixer by opening 9 and 10. Otherwise, pure fuel flowed into the system from the left starting at stem valve 4 and ending in a tube following either valve 16, 17 or 18, depending on the desired tube size. The entire test stand was contained under a ventilated chemical fume hood so that any fuel that escaped the system (in case of leaks) and all exhaust gases were ventilated outside the building.

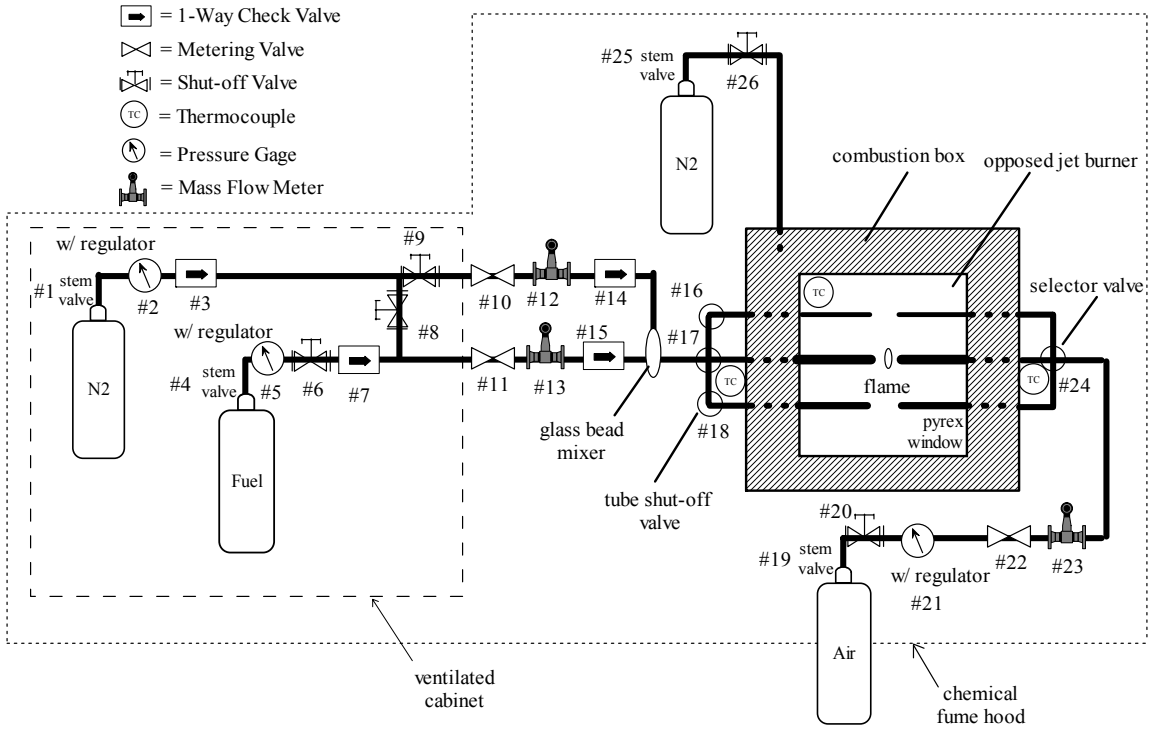

Figure 5.1. Gaseous fuel opposed jet burner test schematic.

5.1.2 Gaseous Test Procedure

Before initial operation of the OJB test stand, the system was checked for leaks by cold flowing the nitrogen, fuel and air and testing all connections. Next, each of the flow

meters (12, 13 and 23) was checked for calibration by flowing air through them as they were connected in series. The final step prior to operation was to obtain highly accurate diameter measurements of the tubes from which the gas entered the OJB. This measurement was taken using pin gages to achieve an accuracy of tenths of a millimeter, with estimates made to the nearest hundredth of a millimeter. The importance of this parameter was revealed in calculations of global strain rate.

The test operation of the gaseous fuel procedure was performed in three basic modes: the initial condition where safety checks and nitrogen purge occurred, the operating procedure where combustion data were taken, and the shutdown procedure where the system was shutdown and purged again with nitrogen. These steps are described in detail as follows.

5.1.2.1 Gaseous Test Initial Condition

The initial condition started with a check to ensure that all valves and regulators were closed. Next, the combustion containment box was opened and ventilated. The system was purged with nitrogen by opening stem valve 1, then purge valve 8, metering valve 11, and tube shutoff valve 16, 17, or 18. The operating pressure of nitrogen was set on regulator 2 to read about 40 psig. Next the valves 8 then 11 were closed and the system was ready to follow the operating procedure.

5.1.2.2 Gaseous Test Data Collection

Operation began by opening the air and fuel stem valves 19 and 4. Then the nitrogen, air, and fuel shutoff valves 9, 20, and 6 were opened allowing gas to flow to the metering valves. Tube size was selected on the fuel side of the box by opening either valve 16, 17, or 18 while the other two remain closed. The corresponding air tube size was selected by a three-way selector valve (24). Next, fuel and air were allowed to flow into the combustion box by opening the metering valves 11 and 22 to a flow of about 0.5 standard liters per minute (SLPM), and a flame was ignited via a hand-held propane torch (not pictured). For safety purposes, if ignition did not occur within one minute, all fuel valves were closed, starting with the stem valve and working towards the OJB, and potential problems were investigated. Once a flame was present, it was centered between the tubes by adjusting the fuel and air metering valves (11 and 22).

At this time the combustion box (with dimensions of about 12×12×10 inches) was covered with a lid that had a wire mesh section (about 4×4 inches), which allowed the exhaust gas to be vented out through the chemical fume hood. Next, the nitrogen bath gas was turned on by opening valves 25 and 26 to about 0.5 SLPM to purge and continuously ventilate the combustion box. Various size wire mesh exhaust openings and nitrogen bath gas flow rates were examined. Numerous repeat experiments with a range of ventilation rates showed that the chosen rates had a negligible affect on extinction limits. The chosen mesh size for ventilation and bath gas flow rate was such that the secondary flame in the combustion box was minimized while the primary opposed flame could be centered without being anchored to either jet. The disk-shaped flame at extinction typically formed a ring-shaped flame that could be restored as opposed to blowing out altogether.

At this point the fuel pressure regulator was checked to read about 25-30 psi and the fuel/nitrogen cabinet door was closed for safety. The nitrogen metering valve 10 was opened if desired to dilute the fuel flow, but remained closed for testing pure fuel. Flow rates were slowly increased using their respective metering valves until extinction was achieved. At extinction the flow rates, internal box temperature, atmospheric pressure, and any pertinent comments were recorded for future analysis. Finally, fuel and air flow rates were reduced until the flame restored, and data were again collected.

5.1.2.3 Gaseous Test Shutdown

To shut the system down, first the fuel stem valve was closed. When the fuel regulator 5 read 0 psig, the nitrogen purge valve 8 was opened and the system was purged of fuel. When the purge was complete, valve 8 was closed, followed by nitrogen and air stem valves 25, 1, and 19. The stem valves were closed first to ensure that there was no pressure remaining in the lines. When the pressures read zero, shutoff and metering valves (9, 10, 6, 11, 20, 22, and 26) were closed, always starting from the source and moving inward towards the OJB. The shutdown procedure concluded testing of each individual gas.

5.2. Liquid Fuel Test Configuration and Procedure

5.2.1 Liquid Test Configuration

The liquid fuel test setup, Figure 5.2 (symbols key shown in Figure 5.1), was the same as the gaseous fuel test setup on the right half of the combustion box and OJB, including the air supply tank and airside tube, and the nitrogen bath gas. On the airside, only the 7.5 mm tube was used for the liquid fuels, so the selector valve (20) always remained in that position. The left side of the figure where fuel entered the combustion box was modified to heat and evaporate the liquid fuel prior to entering the OJB.

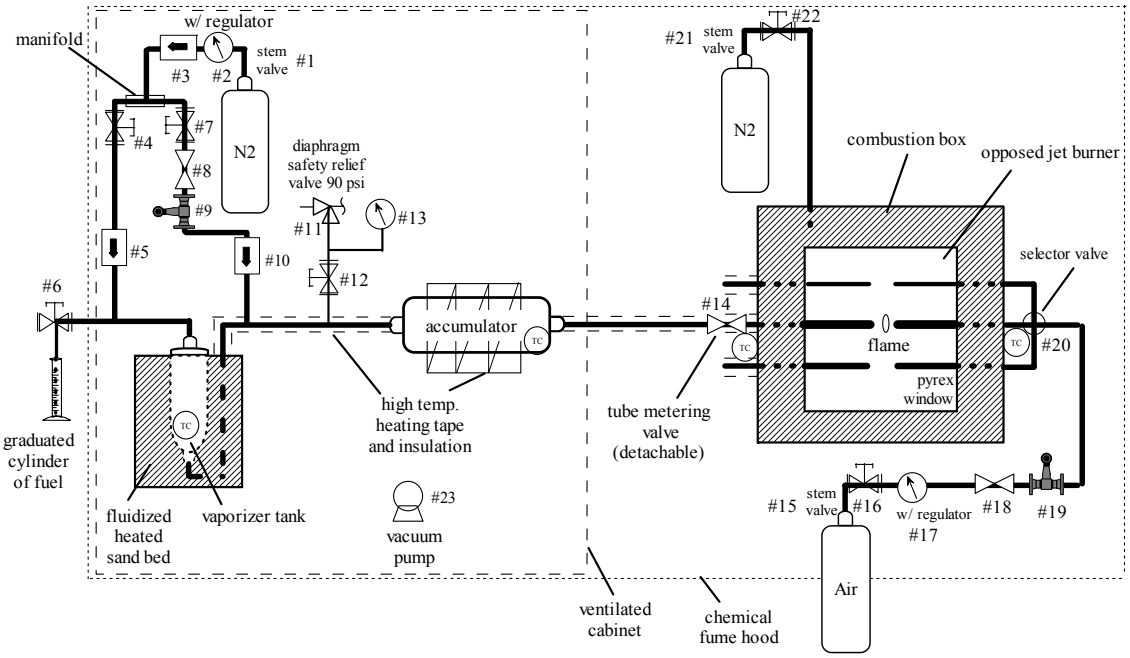

Figure 5.2. Liquid fuel opposed jet burner test schematic

5.2.2 Liquid Test Procedure

As with the gases, the liquid test procedure consisted of initial, operating, and shutdown procedures. Also, it was preceded by an overall system leak check.

5.2.2.1 Liquid Test Initial Condition

The initial condition started with all valves and regulators closed. The combustion box was opened and ventilated. The nitrogen stem valve 1 was opened, followed by the nitrogen shutoff valve 4. The fuel system was purged by opening the

tube metering valve 14. Nitrogen tank pressure was set to about 40 psig. After sufficient purge time, the nitrogen stem and tube valves were closed, followed by the metering valve 14. Next the (10.92 L) closed vaporizer system was evacuated by attaching a separate vacuum pump (23) to shutoff valve 6, which was unattached from the preloaded graduated cylinder of fuel at that time. Valve 12, which protects pressure gage 13 from reaching low pressure, was closed prior to evacuation. The system was then evacuated to near 0 mm Hg. Typical values of system pressure after evacuation ranged between 1 to 5 mm Hg. The system was isolated from the vacuum pump by closing valve 6. The system was ready for operation at this point.

5.2.2.2 Liquid Test Data Collection

The operating procedure began by attaching the fuel line from the graduated cylinder to shutoff valve 6. Unlike the schematic, the graduated cylinder actually sat above valve 6 and liquid fuel was drawn into the system through a drain valve on the bottom. This was done so the tube was not submerged into the liquid fuel, which would have caused the volume graduations on the cylinder to read incorrectly. The amount of liquid fuel desired was pre-calculated using the initial operating pressure and temperature with the equation of state (where system volume was 10.92 L) [49]:

$$pV = znR_uT \tag{5.1}$$

Because the system was closed as the fuel was heated, the volume remained constant, so the only unknown variable was the number of moles of fuel to be added for the pure fuel case. When nitrogen dilution was desired, the amounts of liquid fuel and gaseous nitrogen were pre-calculated by iteratively varying those two quantities to determine what mole fraction of fuel and what operating pressure would be obtained. The gaseous nitrogen was added to bring the system to a predetermined pressure after the liquid fuel was added, and prior to heating the system. The nitrogen diluent was added by opening stem valve 1, shutoff valve 7 and metering valve 8. Pressure due to nitrogen addition was monitored by opening shutoff valve 12 to utilize pressure gage 13 after sufficient time for the system pressure to reach at least 5 psia (259 mm Hg), so as not to damage the pressure gage. Valves 1, 7, and 8 were closed after the desired amount of nitrogen diluent was added.

Once liquid fuel and, if desired, nitrogen diluent were in the closed system, the fluidized, heated sand bed and the high temperature heating tapes were energized, and the system was slowly brought up to operating temperature and pressure. Tests were performed using a blowdown method where the high-pressure, vaporized fuel was allowed to exit the system through metering valve 14 during operation. In the cases of *n*-heptane and JP-10, tests started at a pressure of about 50 to 60 psia (2586 to 3103 mm Hg) and an average system temperature of about 250ºC, which was well above their boiling points, 98ºC and 182ºC respectively at one atmosphere [10,50]. JP-7 was tested at about 350ºC and about the same initial pressure as the other liquid fuels. JP-7 has a boiling point range at atmospheric pressure of 150 to 300ºC, which may vary depending on the particular batch of hydrocarbon mixture [15,51-53].

After the operating temperature and pressure were reached, and the ratio of pressure to average temperature had attained a maximum value, experiments were performed as before in the gaseous fuel test setup in which a flame was centered between the two tubes as fuel and air flow rates were increased until extinction was reached. The delivered fuel flow rate in the liquid fuel test configuration was not monitored as in the gaseous fuel setup because flow meters did not have the capability of operating at the high temperatures and low flows required. Also, although the fuel metering valve in the liquid fuel experiments was specially made to operate under such high temperatures, it was slightly less sensitive than the gaseous fuel metering valves, causing a greater difficulty in keeping the flame centered. The results of this experimental difficulty are discussed further in the following chapter.

5.2.2.3 Liquid Test Shutdown

The shutdown procedure started by opening the metering valve 14 all the way to bleed off the excess fuel while maintaining a flame in the combustion box, until pressure gage 13 read atmospheric pressure. Next the nitrogen stem valve 1 and metering valve 4 were opened to purge the system. A flame was still maintained in the burner as the nitrogen purged the remaining fuel from the system for safety reasons. After sufficient purge time, the sand bed heater and heating tapes were turned off and unplugged. Next, air was attached at shutoff valve 6 and allowed to flow through the system until it reached

ambient temperature. Nitrogen bath gas and purge gas were shutoff by closing stem valves 1 and 21 and shutoff valves 4 and 22. At this point the experiment was complete and the test facility was safely shutdown, concluding the liquid fuel test.

Chapter 6

RESULTS AND DISCUSSION

The experimental setup just described was employed to obtain extinction limit data for hydrogen and eight hydrocarbon fuels. Fuels included gaseous hydrogen, methane, ethane, propane, butane, and ethylene, and liquid *n*-heptane, JP-7, and JP-10. The *n*-heptane and JP-7 experiments were the focus of the investigation. The other fuels were included for shakedown tests of the apparatus, for comparison of the results with data from the literature, and to obtain a relative reactivity scale for a broad classification of fuels. Following are results showing the effect of the opposed jet burner tube size, a comparison with available data from other investigations with nozzle and tube setups, and the new data for the *n*-heptane and JP-7.

6.1 Tube Size Comparisons

Extinction limit data were taken using three to four tubes of different diameters for the following pure fuels: methane, ethane, ethylene, and propane. The goal of testing different tube sizes was to verify that U_{air}/D_t at extinction approached a constant value as size and flow rate at extinction increased. The four nominal tube diameters tested were 2.9, 5.0, 7.5, and 9.3 mm, and the resulting data are shown in Figure 6.1. The ethylene was not tested in the 9.3 mm tube because the flow of ethylene would have been turbulent at the largest tube diameter, and these were all laminar flame experiments. There are data shown for *n*-heptane, JP-7, JP-10, and butane in the single tubes in which they were tested, for comparison to the other fuels.

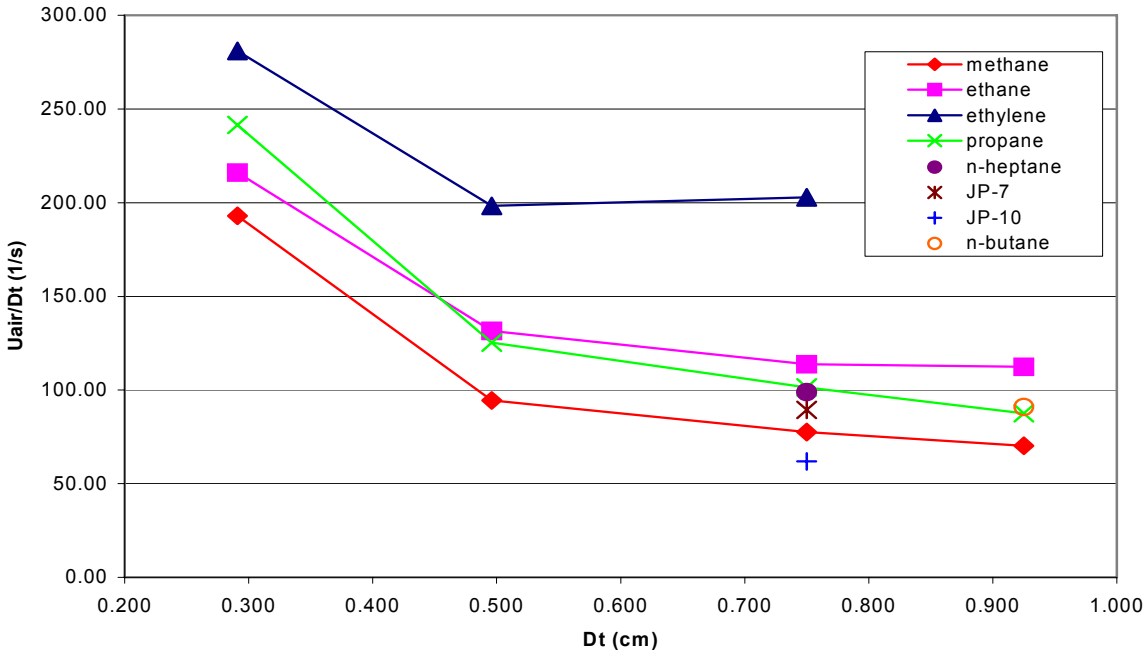

Figure 6.1. U_{air}/D_t using tubes of varying diameters for several hydrocarbon-air systems.

As presented in Figure 6.1, when tube diameter is reduced from 2.9 mm to 5.0 mm, the decrease in U_{air}/D_t is quite large. From 5.0 mm to 7.5 mm the difference is much smaller, and even more so from 7.5 to 9.3 mm. In the case of ethylene the difference between 5.0 mm and 7.5 mm is less than 2%, and therefore is assumed negligible, showing that U_{air}/D_t has reached a constant for ethylene in the larger tubes. Also, for ethane in the 7.5 and 9.3 mm tubes the difference is about 1%, where it has essentially reached a constant value. A table of average values of U_{air}/D_t for each of the fuels in each tube size is given in Appendix A. The tendency for U_{air}/D_t to approach a constant for larger tube diameters is due to flatter, relatively thinner, more closely one-dimensional, ideal flames with reduced edge effects occurring at the higher flow rates required to cause extinction in a larger tube size. This demonstrates clearly that higher flow rates and therefore higher Reynolds numbers based on tube diameter are desirable, yet it is important that the flow remain laminar to ensure the physical simplicity and universal repeatability of a laminar flame study [16,20,33]. For a circular tube with fully developed flow, Reynolds numbers are less than about 2100 [47]. Table 6.1 provides Reynolds numbers calculated from the equation [10,47,49]:

$$\frac{D_t U_{fuel} \rho}{\mu} \tag{6.1}$$

for each of the gaseous hydrocarbon fuels in the 5.0, 7.5, and 9.3 mm tubes, as well as hydrogen in the 2.9 mm tube and *n*-heptane and JP-7 in the 7.5 mm tube. (Hydrogen was not tested in the larger tubes because its very rapid combustion required air flows for extinction that would exceed the range of the flow meters.) Density was determined using the ideal gas equation, and values of dynamic viscosity were calculated using temperature dependent equations [54,55]. In the case of gaseous fuels, fuel volumetric flow rate was recorded via flow meter and used to determine U_{fuel} by dividing by cross-sectional area and multiplying by the flow meter factor for a given fuel. For the liquid fuels, namely *n*-heptane and JP-7, fuel flow rate could not be measured because the fluid was too hot and moving at a flow rate below that which any flow meter could measure. Therefore, U_{fuel} was determined recognizing that there was an axial momentum flux balance between the air and fuel streams, where the flame was assumed to be perpendicular to the axis, yielding the equation [10,31,37,38]:

$$(\dot{m}U)_{air} = (\dot{m}U)_{fuel} \tag{6.2}$$

Flow adjustment and flame centering produced this condition as part of the experimental procedure. In this case, the axial (1-D) momentum flux balance is represented by the equation:

$$\left(\rho U^2\right)_{air} = \left(\rho U^2\right)_{fuel} \tag{6.3}$$

because the tube exit areas are the same.

Table 6.1. Reynolds numbers for various fuels in different diameter tubes.

Fuel	2.9 mm	5.0 mm	7.5 mm	9.3 mm
Hydrogen	530			
Methane		110	300	429
Propane		500	1160	1355
Ethane		490	1060	1466
Ethylene		740	1720	
n-Heptane			940	
JP-7			940	

As Table 6.1 and Figure 6.1 show, based on the results for ethylene and ethane in particular, all of the fuels in the larger tubes are at Reynolds numbers that provide data in the range where U_{air}/D_t is nearing a constant.

6.2 Current versus Previous OJB Data Comparisons

6.2.1 Hydrogen Study: Previous versus New Data

Previous OJB systems at NASA Langley Research Center have been verified using numerical analysis and analytical modeling. Therefore, a critical step in establishing this new OJB test setup was to show a comparison to the previous OJB analytical and experimental data obtained at NASA Langley employing a different apparatus [1,2]. Pure hydrogen was the chosen fuel for this purpose because of its extensive use in the past. The key parameter for finding extinction limits is U_{air}/D_t because it is proportional to the global strain rate as shown previously. Results from the current system give an average U_{air}/D_t of 2130 1/s normalized to 300K and atmospheric pressure. Previous experimental data using a 2.7 mm tube yielded an average U_{air}/D_t of 2050 1/s [1]; these data are in excellent agreement, with a difference of less than 4%. Two-dimensional numerical simulations using parabolic inflow boundaries give a U_{air}/D_t of 2150 1/s, which is within 1% of the current data [2]. These results provide an excellent baseline for the new test equipment.

6.2.2 Propane Study: Gaseous versus Liquid Test Configuration

Once the gaseous fuel test setup was validated, it was important to compare results from it with the liquid fuel configuration that would be used to take JP-7 and *n*-heptane data. An experiment was performed with propane that helped establish the liquid setup in two ways. First, a test was performed using propane in a heated, batch mode, just as was done with the liquid fuels, reaching similar temperatures and pressure. The fuel that had been heated for about 2 hours was then tested for extinction limits using the 7.5 mm tube. Next, the propane was flowed directly through the liquid system in a continuous mode while it was still hot to show the effects that heating in a closed system had on the fuel. The resulting extinction limits are given in Table 6.2. The extinction limits were slightly higher (about 3.4%) for both of the heated fuels, as expected due to

increased fuel diffusion and reactivity at input temperatures, and therefore increased Damköhler number and slightly shorter chemical reaction time [10,29,56]. The difference is small enough to indicate that (1), the liquid system compares very well with the gaseous system and does not show evidence of thermal cracking of the fuel, and (2), heating of fuel does not affect the extinction limit significantly. Therefore, it is appropriate to compare the heated hydrocarbon fuel extinction limit data to the ambient gaseous fuel data without including a correction factor.

Table 6.2. Comparison of propane tested in the gaseous fuel setup to the liquid fuel setup using a batch method and a continuous flow method.

Fuel	Uair/Dt at extinction	% difference from heated batch method
C3H8	101.4	-3.0
Heated C3H8 batch	104.4	0
Heated C3H8 continuous flow	105.2	0.8

The data in Table 6.2 for the heated propane in a batch mode and in a continuous flow mode are statistically the same. This leads to the conclusion that the combustion behavior of the fuel is not adversely affected by the closed system heating process.

6.2.3 Nozzle versus Tube Study

Another important comparison between previous OJB systems and the present OJBs is the effect of using a straight tube versus a tapered nozzle. Several fuels were tested for this purpose including hydrogen, methane, ethane, ethylene, and propane, all of which are shown in Figure 6.2, except for hydrogen. Hydrogen is omitted for two reasons; first, it has such high flame strength relative to the other fuels that U_{air}/D for hydrogen is well off of this chart for both a tube and nozzle, causing the other data points to become indiscernible on the plot when included. The second reason is that hydrogen follows a slightly different trend in which U_{air}/D_t is about three times U_{air}/D_n [1]. For just the gaseous hydrocarbons tested, U_{air}/D_t is about 2.55 times U_{air}/D_n as shown by the slope of the curve fit line in Figure 6.2. This constant of proportionality appears to be more

appropriate for hydrocarbons due to the closer location of the flame zone to the stagnation surface; and thus it was used to determine the equivalent strain rate for *n*-heptane and JP-7 below.

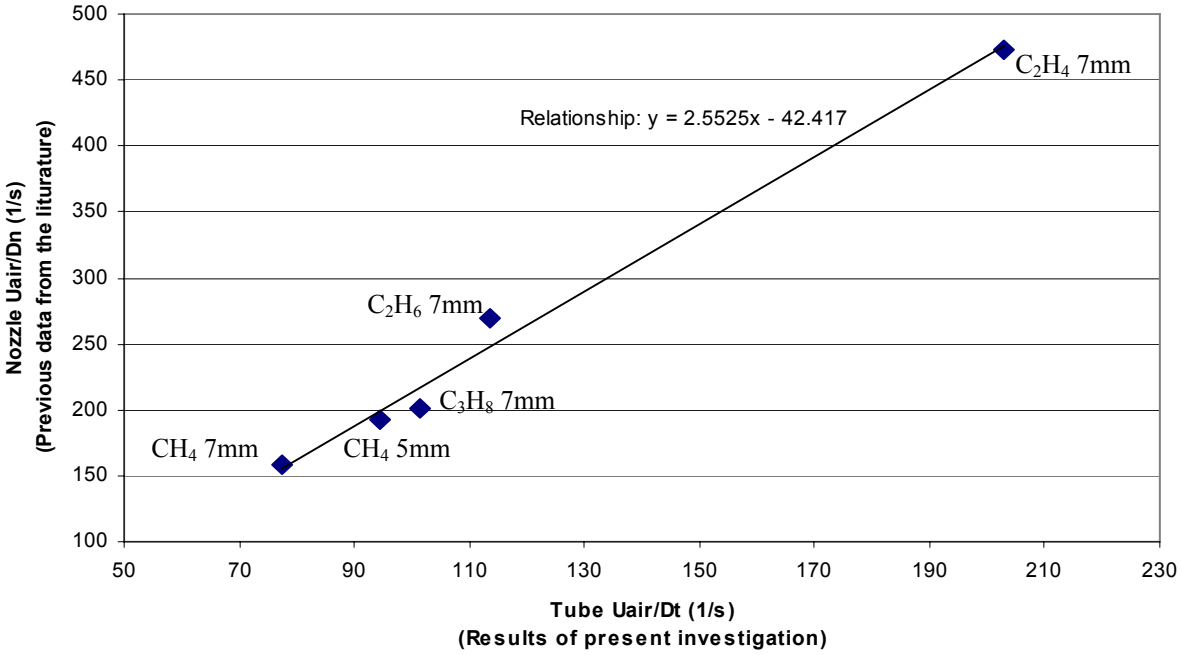

Figure 6.2. Relationship of nozzle versus tube opposed jet burner extinction limits.

6.3 JP-7 and *n*-Heptane Results

6.3.1 JP-7 Molecular Weight and Compressibility Factor Calculation

In order to evaluate nitrogen-diluted JP-7 extinction limits, it is necessary to first determine the molecular weight to compressibility factor ratio. This ratio is required in calculating the mole fraction of JP-7 in nitrogen for a given test, and for estimating the Reynolds number. The ratio, referred to as MW/z, was found in this experiment by heating a known quantity of pure JP-7 fuel until it was fully vaporized in the closed system, and recording system pressure and temperatures. As the system was closed and the fuel was heated, it was found that the system had a slow leak, based on a decrease in the ratio of pressure to average temperature after the fuel had been fully vaporized. Without a leak this ratio would have remained constant over time, as provided in the equation of state (5.1). In this case the other parameters: compressibility, volume, total moles of gas, and the universal gas constant would all remain nearly constant once the

liquid fuel was vaporized. Figure 6.3 provides pressure to average temperature ratio versus time lapsed for three separate experiments with pure JP-7. Note the absolute lapsed time for each experiment is somewhat arbitrary because of the designation of time zero, and the subsequent ramping-up of heater temperatures was different in each case.

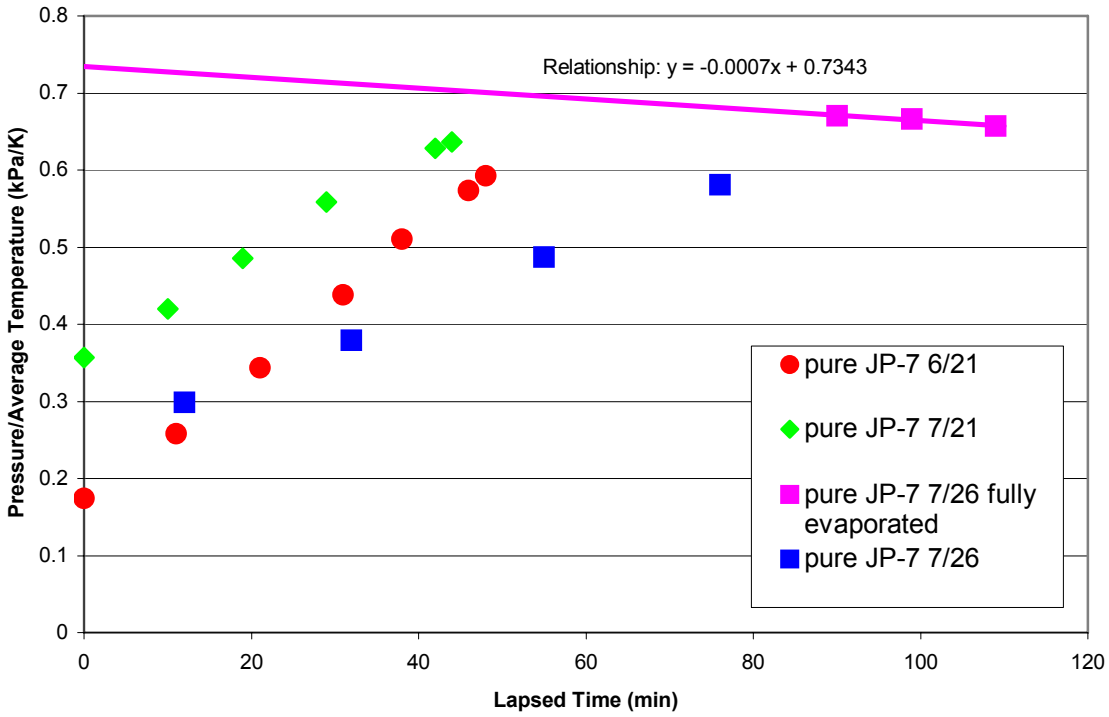

Figure 6.3. Rate of change of system pressure to average temperature ratio used for JP-7 molecular weight/compressibility factor calculation.

The data show that only during the experiment on July 26th was total vaporization of the fuel clearly confirmed, because in the other cases pressure over average temperature continued to increase as the fuel was still evaporating, and a downward trend was not documented. Extensive amounts of data were recorded and plotted similarly for *n*-heptane and JP-10 fuels in the closed system, and the leak rate found for the July 26th case of JP-7 was approximately consistent with these data. Therefore, this case is used to evaluate MW/z using the equation of state for the closed system and correcting for the leak as follows. A straight line is drawn through the last three points of the 7/26 data, which show a consistent decrease in pressure/temperature ratio, as was also found in

numerous previous tests. The line is extrapolated back to the vertical intercept of the graph, at the time when evaporation of the fuel started. It is assumed that the system leak was constant starting from this approximate time. The corrected pressure/temperature ratio for the initial amount of liquid fuel in the cold system is thus assumed to represent complete evaporation in the absence of system leak. Therefore it is this ratio that was used in calculating MW/z in a modified equation of state:

$$\frac{MW}{z} = \frac{mR_u T}{pV} \tag{6.4}$$

where m is the mass of JP-7 found by multiplying its liquid density by the volume of fuel added to the system. The resulting MW/z calculated was 181 g/mol for a system pressure of about 60 psia.

6.3.2 *n*-Heptane and JP-7 Extinction Limits

The results of the extinction limit experiments for *n*-heptane and JP-7 are presented in Figures 6.4 and 6.5. The strain rate at extinction was calculated by first multiplying U_{air}/D_t by 2, as was found from the plug flow approximation of a nozzle, then multiplying by 2.55 which was the determined factor of proportionality for a hydrocarbon fuel from Figure 6.2, giving a final global strain rate equal to $5.1U_{air}/D_t$.

Figure 6.4 shows the data with ±1 standard deviation bars for experiments with varying mole fractions *n*-heptane and JP-7. Pure JP-10 fuel is included for comparison, but *n*-heptane and JP-7 remain the focus of this study. As shown, there is a significant spread in the strain rates, particularly at the smaller mole fractions. It was found that the strain rate at extinction increased systematically as an experiment progressed, suggesting that the (mostly) diffusional mixing of fuel and nitrogen was probably not complete, as the percentage fuel and corresponding strain rate appeared to increase slightly over time. Another contributor to data spread was the less sensitive metering valve required for the high temperature flows as mentioned previously. The flame was easier to center between the tubes at lower pressures as the system blew down. Since the data were ultimately averaged, as seen in Figure 6.5, this imperfect mixing and metering valve control difference is believed to have little effect on the final results.

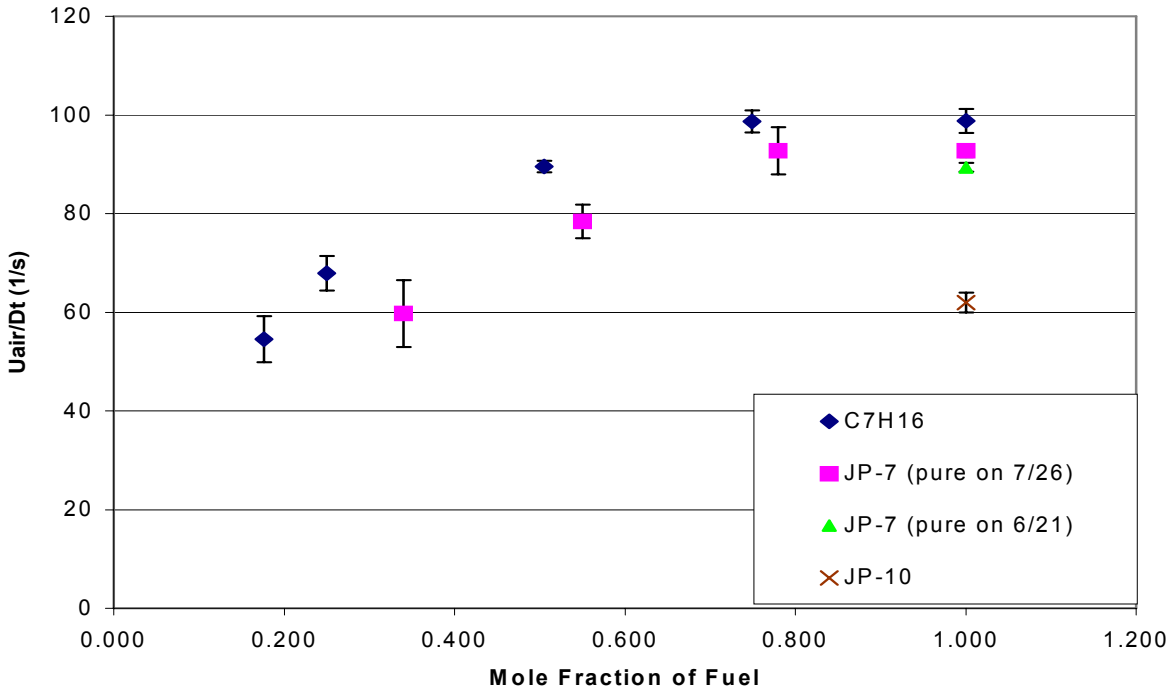

Figure 6.4. Variability of *n*-heptane, JP-7 and JP-10 extinction limit data at various mole fractions in nitrogen.

Results for pure JP-7 from two separate experiments on June 21st and July 26th are shown in Figure 6.4. The results from the first experiment gave a slightly lower extinction limit, which was also below that of the 78% JP-7. This may be due to incomplete vaporization of the JP-7 fuel, as is evident in Figure 6.3. Therefore, the data taken on July 26th is used in the final result plotted in Figure 6.5.

Extinction limits, as well as restoration limits, where the ring flame formed at extinction reformed a disk flame as the flow rates were lowered, are given for *n*-heptane and JP-7 in Figure 6.5. The numerical data are provided in Appendix B. The restoration data appear less consistent than the extinction data, and does not follow quite the same curve that is typical of extinction limits. This may be due in part to fewer data points being recorded at restoration, because it was not always achievable. When the flame blew out at extinction, most often it formed a ring flame that could be restored at lower flow rates, but sometimes it blew out all together and no restoration was recorded.

Figure 6.5 also shows the hysteresis between blowoff and restoration, which has been observed previously for gaseous hydrocarbons and hydrogen [1,16,22]. The

occurrence of hysteresis is an important characteristic to consider for combustor applications. When a hydrocarbon or hydrogen flame undergoes strain induced extinction, it will not usually relight until a significantly lower flow rate is reached [1]. (The relative hysteresis for hydrogen and several hydrocarbon fuels is shown in Figure 6.6 where all of the tested fuels are compared.)

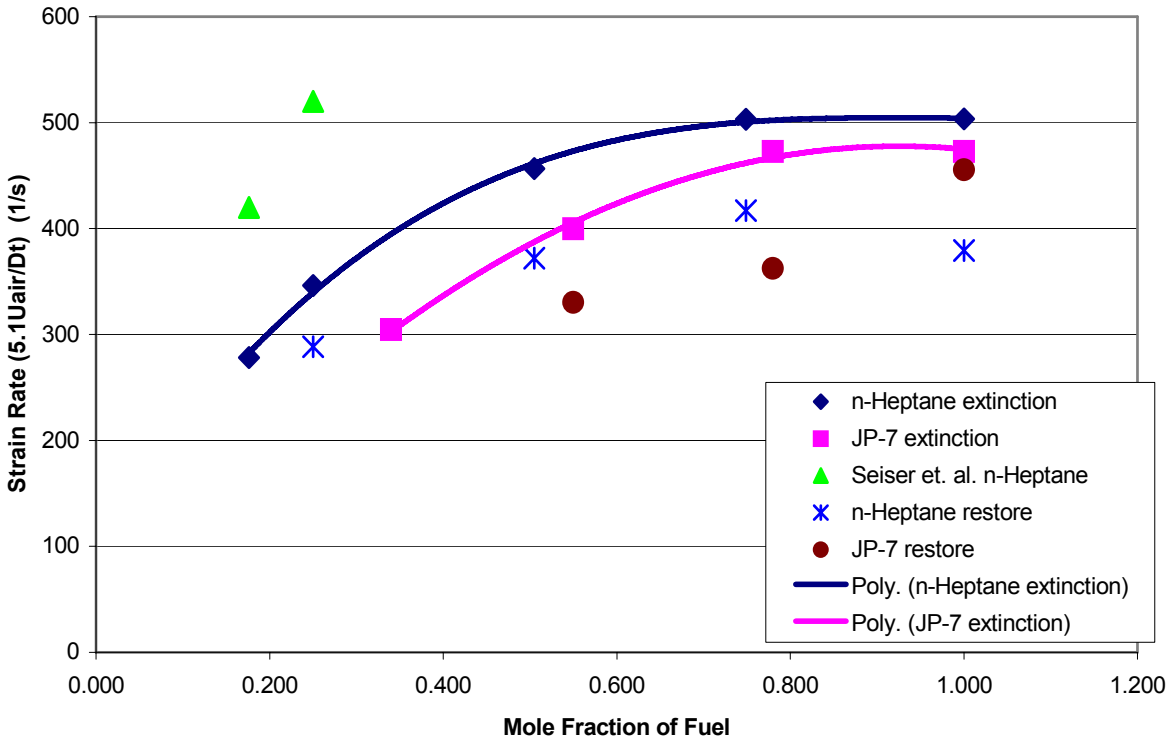

Figure 6.5. Strain rate at extinction and restoration for *n*-heptane and JP-7 at varying mole fractions.

Also provided in this plot are extinction data for 0.25 and 0.18 mole fractions of *n*-heptane in nitrogen found by Seiser, *et al* [38]. The previous data are notably higher than the new data, showing greater than a 30% difference. However, the methodologies differ as well, where Seiser, *et al* use a large diameter matrix OJB of about 22 mm and a small tube separation of about 10 mm, which alters the strain rate equations as shown previously. Similar differences have been seen in past studies with hydrogen extinction limits [1,57,58]. More importantly, this apparent 40% discrepancy in data was clearly demonstrated by the experimental (LDV) measurements of Rolon, *et al* [36]. They

demonstrated, using air versus air jets, that a larger spacing of matrix nozzles (at least one and a half diameters as used in this study) yielded global strain rates that agreed with measured strain rates. The much smaller spacing gave significantly higher results (approximately 40%) [36].

The shape of the data curve for both *n*-heptane and JP-7 experiments is similar, and as expected, strain rate at extinction increases as mole fraction increases, approaching a horizontal asymptote as a mole fraction of one is reached. The data are provided in Appendix B.

The final presentation of data is a comparison of extinction and restoration limits for all of the fuels used in this research, given in Figures 6.6 and 6.7. In Figure 6.6 the vertical axis is plotted on a logarithmic scale, and in Figure 6.7 it is plotted on a linear scale without hydrogen to show more detail of the other fuels. These plots demonstrate that the hysteresis between blowoff and restoration can be quite large, as in the cases of hydrogen and ethylene. Figure 6.6 shows that the flame strength of hydrogen relative to the hydrocarbon fuels is extremely high, and so it is best compared using the log scale. JP-10 was the weakest fuel tested, and no restorations were recorded for it. Most of the data presented were taken with a 7.5 mm tube, with the exceptions of hydrogen and butane. The hydrogen, as previously stated, cannot be tested in the larger tube sizes, and the butane was only tested in the largest tube due to time constraints. Figures 6.6 and 6.7 help to illustrate the relative reactivity scale for all of the fuels, which is important for practical applications in combustor design.

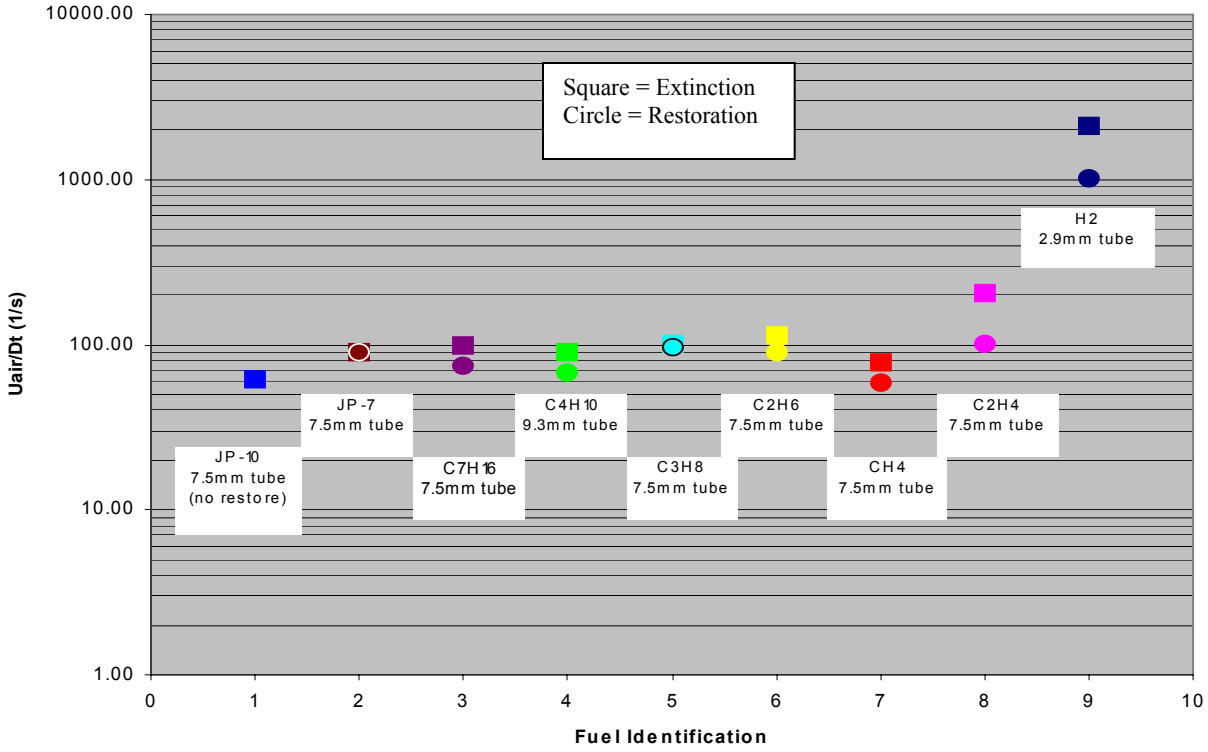

Figure 6.6. Average extinction and restoration limits for hydrogen and several hydrocarbon fuels in varying tube sizes on a logarithmic scale.

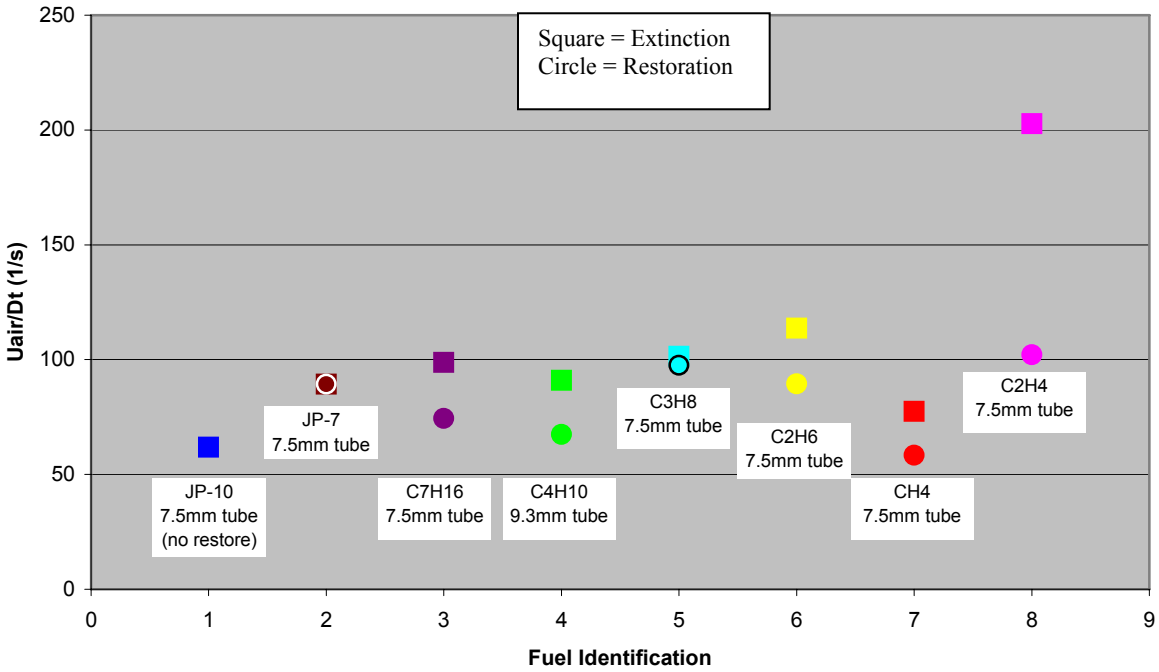

Figure 6.7. Average extinction and restoration limits for several hydrocarbon fuels in varying tube sizes on a linear scale.

Chapter 7

CONCLUSIONS

New opposed jet burner (OJB) and liquid fuel vaporizer systems were constructed, several tasks were completed to validate the new systems, and unique OJB extinction data were obtained. The effect of OJB tube diameter on extinction limits was demonstrated in a series of experiments using four different diameter tubes. Next, the gaseous system was validated through hydrogen-air extinction experiments that compared remarkably well with previous studies, and the liquid configuration was validated with the gaseous setup in a three-part experiment with propane. Nozzle and tube OJB data were compared to establish a constant of proportionality between the data utilized in calculating extinction limits. Finally, new *n*-heptane and JP-7 extinction limit data were successfully obtained over a wide range of fuel concentrations (18 to 100 mole %) with nitrogen diluent, and an approximate value of JP-7 molecular weight to compressibility factor ratio was calculated. These data were the principal objective of the research effort, which was considered successful in producing new and unique results of interest to the high-speed combustion community.

In the varying tube size experiments, it was shown that for laminar flow, the strain rate at extinction (proportional to air velocity normalized by tube diameter) approaches a constant value as tube diameter increases, due to the flame decreasing in thickness/diameter ratio and approaching one-dimensionality. This was demonstrated using methane, ethane, propane, and ethylene in tubes of 2.9, 5.0, 7.5, and 9.3 mm diameter (all but the largest size for ethylene). Particularly for ethylene in the 5.0 to 7.5 mm tube and ethane in the 7.5 to 9.3 mm tube, the air velocity divided by tube diameter reached a constant value while still maintaining laminar flow (Figure 6.1). The other fuels followed the same trends and were nearing a constant as the tube diameter increased.

Next the results from the gaseous fuel system were compared to previous experimental studies as well as 2-D numerical simulations using pure hydrogen, yielding comparative results within 4% and 1% respectively. This excellent agreement using the smallest tubes provided a baseline for the system overall. Following the hydrogen

experiment was a test to compare results from the gaseous setup to the liquid fuel setup, which typically required heating and evaporating the fuel prior to testing it in the OJB. Gaseous propane was the chosen fuel for this system comparison, yielding several important results. First, the propane was heated in the closed liquid setup to temperatures and pressure similar to those used for *n*-heptane, JP-7, and JP-10. The extinction limit data using this batch method were only about 3% higher than the data found using the gaseous setup. It was expected that the results would be a bit higher with preheated fuel due to enhanced fuel diffusion and reactivity caused by increased temperature. Thus the liquid setup appeared to produce data that compared well with the gaseous setup and did not show gross evidence of propane decomposition. The data were close enough that a correction factor due to preheating did not appear to be needed for the liquid *n*-heptane, JP-7 and JP-10 data. Next, the propane was flowed through the hot liquid test setup in a continuous flow method to compare with the batch method and determine if long-term pyrolysis of propane had any measurable effect. The resulting data were essentially the same, leading to the conclusion that the batch heating process did not alter the fuel characteristics.

Following the hydrogen and propane studies, several hydrocarbons were tested and compared to data from an OJB using 7.2 mm contoured Pyrex nozzles instead of straight tubes. The results yielded a constant of proportionality between the two (2.55), as shown in Figure 6.2, which allowed for axial strain rate to be calculated for all hydrocarbons tested in the tube setup.

Finally, new *n*-heptane and JP-7 extinction limits were presented in Figures 6.4 and 6.5. Data ranged from 0.18 to 1.0 mole fraction of *n*-heptane in nitrogen, and 0.34 to 1.0 mole fraction of JP-7 in nitrogen. The 18% and 26% *n*-heptane data were in essential agreement with published data, obtained with a 22 mm matrix-type OJB at low mole fractions in nitrogen by Seiser, *et al* [38] *if* one accepts Rolon's LDV strain rate measurements [36] that the close nozzle spacing in [38] produces results that are about 40% high. Both the *n*-heptane and JP-7 data curves followed the trends of hydrogen and other hydrocarbons, where the extinction limits increased with increasing mole fraction and approached asymptotic values as a mole fraction of one was approached.

There is a wealth of future work that can be done with the new OJB gaseous and liquid test configurations, both with the current fuels under study and with new fuels. Some suggestions for future JP-7 experiments in the OJB include similar tests for catalytically cracked JP-7 fuel, or using JP-7 with fuel additives. Another desirable experiment is to develop a surrogate fuel for JP-7 that is a precise and consistent mixture of hydrocarbons for the sake of repeatability and model ability to test finite rate kinetics and reduced kinetic schemes. It is also of interest to test JP-7 in a combustor utilizing Scramjet ignition and flame holding aids such as a plasma torch or pyrophoric additives like silane or triethylaluminum. Other fuels for which the new OJB system can be employed include JP-10 at varying mole fractions, previously tested fuels with additives, and other common hydrocarbon fuel (perhaps JP-8, JP-4 or Jet-A) for which there are various practical applications.

APPENDIX A

Table A1. Average U_{air}/D_t (1/s) at 300 K and 1 atm in tubes of various best-estimate inside diameters.

Fuel	2.91 mm	4.96 mm	7.50 mm	9.25 mm
Hydrogen	2131			
Methane	193	94	78	70
Ethane	216	132	114	112
Ethylene	281	198	203	
Propane	241	125	101	88
n-Heptane			99	
JP-7			93	
JP-10			62	

APPENDIX B

Table B1. Strain rate at extinction and restoration (1/s) at 300 K and 1 atm for various mole fractions of fuel in nitrogen.

Fuel	Mole Fraction	Strain Rate at Extinction	Strain Rate at Restoration
n-Heptane	1.00	99	74
	0.75	99	82
	0.51	90	73
	0.25	68	57
	0.18	55	-
JP-7	1.00	93	89
	0.78	93	71
	0.55	78	65
	0.34	60	-

REFERENCES

(1) Pellett, G. L., Isaac, K. M., Humphreys, W. M., Jr., Gartrell, L. R., Roberts, W. L., Dancey, C. L., and Northam, G. B., "Velocity and Thermal Structure, and Strain-Induced Extinction of 14 to 100% Hydrogen-Air Counterflow Diffusion Flames," *Combustion and Flame*, vol. 112, 1998, pp. 575-592.

(2) Hwang, K. C., "Two Dimensional Numerical Simulation of Highly-Strained Hydrogen-Air Opposed Jet Laminar Diffusion Flames," Ph.D. Dissertation, Old Dominion University, May 2003.

(3) Dixon-Lewis, G., "Structure of Laminar Flames," *Twenty-Third Symposium (International) on Combustion*, The Combustion Institute, Pittsburg, 1990, pp. 305-324.

(4) Peters, N., "Laminar Flamelet Concepts in Turbulent Combustion," *Twenty-First Symposium (International) on Combustion*, The Combustion Institute, Pittsburg, 1986, pp. 1231-1250.

(5) Chelliah, H. K., Law, C. K., Ueda, T., Smooke, M. D., and Williams, F. A., "An Experimental and Theoretical Investigation of the Dilution, Pressure and Flow-Field Effects on the Extinction Condition of Methane-Air-Nitrogen Diffusion Flames," *Twenty-First Symposium (International) on Combustion*, The Combustion Institute, Pittsburg, 1986, pp. 503-511.

(6) Potter, A. E., Jr. and Butler, J. N., "A Novel Combustion Measurement Based on the Extinguishment of Diffusion Flames," *American Rocket Society Journal*, vol. 29, 1959, pp. 54-56.

(7) Potter, A. E., Jr., Heimel, S., and Butler, J. N., "Apparent Flame Strength: A Measure of Maximum Reaction Rate in Diffusion Flames," *Eighth Symposium (International) on Combustion*, The Combustion Institute, Pittsburg, 1967, pp. 1027-1034.

(8) Yu, G., Li, J. G., Zhao, Z., Chang, X. Y., and Sung, C. J., "Investigation of Vaporized Kerosene Injection in a Supersonic Model Combustor," *American Institute of Aeronautics and Astronautics*, AIAA-2003-6938, 2003.

(9) NASA Dryden Flight Research Center Photo Collection, http://www.drfc.nasa.gov/gallery/photo/index.html, NASA Photo: ED99-45243-01, 1999.

(10) Turns, S. R., *An Introduction to Combustion: Concepts and Applications, Second Edition*, The McGraw-Hill Companies, Inc., USA, 2000.

(11) Burke, S. P., Schumann, T. E. W., "Diffusion Flames," *Industrial and Engineering Chemistry*, vol. 20, no. 10, 1928, pp. 998-1004.

(12) Tsuji, H., "Counterflow Diffusion Flames," *Energy Combustion Science*, vol. 8, 1982, pp. 93-119.

(13) Zeldovich, Y. B., "On the Theory of Combustion of Initially Unmixed Gases," Translation for *National Advisory Committee for Aeronautics (NACA)*, Technical Memorandum 1296, Washington, June 1951.

(14) Spalding, D. B., *Fuel*, vol. 32, 1953, pp. 169-185.

(15) Otsuka, Y. and Niioka, T., "On the Deviation of the Flame from the Stagnation Point in Opposed-Jet Diffusion Flames," *Combustion and Flame*, vol. 19, no. 2, 1972, pp. 171-179.

(16) Pellett, G. L., Reid, B., McNamara, C., Johnson, R., Kabaria, A., Panigrahi, B., and Wilson, L. G., "Acoustic Weakening of Methane-, Ethylene-, and Hydrogen-Air Counterflow Diffusion Flames, and Implications for Scramjet Flameholding," *American Institute of Aeronautics and Astronautics*, AIAA-2003-4634, 2003.

(17) Pellett, G., Kabaria, A., Panigrahi, B., Sammons, K., Convery, J., and Wilson, L., "Dynamic Weakening (Extinction) of Simple Hydrocarbon-Air Counterflow Diffusion Flames by Oscillatory Inflows," *American Institute of Aeronautics and Astronautics*, AIAA-2005-4332, 2005.

(18) Zhao, J., Isaac, K. M., and Pellett, G. L., "Global Characteristics and Structure of Hydrogen-Air Counterflow Diffusion Flames," Journal of Propulsion and Power, vol. 12, no. 3, 1996, pp. 534-542.

(19) Pellett, G. L., Northam, G. B., Wilson, L. G., Jarrett, O., Jr., Antcliff, R. R., Dancey, C. L., and Wang, J. A., "Opposed Jet Diffusion Flames of Nitrogen-Diluted Hydrogen vs. Air: Axial LDA and CARS Surveys; Fuel/Air Strain Rates at Extinction," *American Institute of Aeronautics and Astronautics*, AIAA-89-2522, 1989.

(20) Pellett, G. L., Roberts, W. L., Wilson, L. G., Humphreys, W. M., Jr., Bartram, S. M., Weinstein, L. M., and Isaac, K. M., "Structure of Hydrogen-Air Counterflow Diffusion Flames Obtained by Focusing Schlieren, Shadowgraph, PIV, Thermometry, and Computation," *American Institute of Aeronautics and Astronautics*, AIAA-94-2300, 1994.

(21) Pellett, G.L., Wilson, L.G., Humphreys, W. M., Jr., Bartram, S.M., Gartrell, L.R., and Isaac, K.M., "Velocity Fields of Axisymmetric Hydrogen-Air Counterflow Diffusion Flames from LDV, PIV, and Numerical Computation," *American Institute of Aeronautics and Astronautics*, AIAA-95-3112, 1995.

(22) Pellett, G. L., Northam, G. B., and Wilson, L. G., "Counterflow Diffusion Flames of Hydrogen, and Hydrogen Plus Methane, Ethylene, Propane, and Silane, vs. Air: Strain Rates at Extinction," *American Institute of Aeronautics and Astronautics*, AIAA-91-0370, 1991.

(23) Pandya, T. P. and Weinberg, F. J., "The Study of the Structure of Laminar Diffusion Flames by Optical Methods," *Ninth Symposium (International) on Combustion*, The Combustion Institute, Pittsburg, 1963, pp. 587-596.

(24) Tsuji, H. and Yamaoka, I., "The Counterflow Diffusion Flame in the Forward Stagnation Region of a Porous Cylinder," *Eleventh Symposium (International) on Combustion*, The Combustion Institute, Pittsburg, 1967, pp. 979-984.

(25) Tsuji, H. and Yamaoka, I., "The Structure of Counterflow Diffusion Flames in the Forward Stagnation Region of a Porous Cylinder," *Twelfth Symposium (International) on Combustion*, The Combustion Institute, Pittsburg, 1969, pp. 997-1005.

(26) Tsuji, H. and Yamaoka, I., "Structure Analysis of Counterflow Diffusion Flames in the Forward Stagnation Region of a Porous Cylinder," *Thirteenth Symposium (International) on Combustion*, The Combustion Institute, Pittsburg, 1971, pp. 723-731.

(27) Smooke, M. D., Lin, P., Lam, J. K., and Long, M. B., "Computational and Experimental Study of a Laminar Axisymmetric Methane-Air Diffusion

Flame," *Twenty-Third Symposium (International) on Combustion*, The Combustion Institute, Pittsburg, 1990, pp. 575-582.

(28) Guerra, R., Pellett, G. L., Wilson, L. G., and Northam, G. B., "Opposed Jet Burner Studies of Effects of CO, CO_2, and N_2 Air-contaminants on Hydrogen-air Diffusion Flames," *American Institute of Aeronautics and Astronautics*, AIAA-87-1960, 1987.

(29) Jain, V. K. and Mukunda, H. S., "On the Ignition and Extinction Problems in Forced Convection Systems," *International Journal of Heat and Mass Transfer*, vol. 11, 1968, pp. 491-508.

(30) Fendell, F. E., "Ignition and Extinction in Combustion of Initially Unmixed Reactants," *Journal of Fluid Mechanics*, vol. 21, 1965, pp. 281-303.

(31) Berta, P., Puri, I. K., and Aggarwal, S. K., "Characteristics of *n*-Heptane/Air N_2 Diluted Counterflow Flames," *American Institute of Aeronautics and Astronautics*, AIAA-2003-1354, 2003.

(32) Hahn, W. A. and Wendt, J. O. L., "Analysis of the Flat Laminar Opposed Jet Diffusion Flame with Finite Rate Detailed Chemical Kinetics," *Combustion Science and Technology*, vol. 27, 1981, pp. 1-17.

(33) Spalding, D. B., "Theory of Mixing and Chemical Reaction in the Opposed-Jet Diffusion Flame," *American Rocket Society Journal*, vol. 31, 1961, pp. 763-771.

(34) Dancey, C. L. and Long, S. R., "Experimental Investigation of the Strain Rate Field in Stretched Laminar H_2/Air Diffusion Flames," *American Institute of Aeronautics and Astronautics*, AIAA-93-3068, 1993.

(35) Cooke, J. A., Bellucci, M., Smooke, M. D., Gomez, A., Violi, A., Faravelli, T. and, Ranzi, E., "Computational and Experimental Study of JP-8, a Surrogate, and Its Components in Counterflow Diffusion Flames," *Proceedings of the Combustion Institute*, vol. 30, 2005, pp. 439-446.

(36) Rolon, J.C., Veynante, D., and Martin, J. P., "Counter Jet Stagnation Flows," *Experiments in Fluids*, vol. 11, 1991, pp. 313-324.

(37) Berta, P., Puri, I. K., and Aggarwal, S. K., "Structure of Partially Premixed *n*-Heptane-Air Counterflow Flames," *Proceedings of the Combustion Institute*, vol. 30, 2005, pp. 447-453.

(38) Seiser, R., Truett, L., Trees, D., and Seshadri, K., "Structure and Extinction of Non-Premixed *n*-Heptane Flames," *Twenty-Seventh Symposium (International) on Combustion*, The Combustion Institute, Pittsburg, 1998, pp. 649-657.

(39) Li, S. C. and Williams, F. A., "Counterflow Heptane Flame Structure," *Proceedings of the Combustion Institute*, vol. 28, 2000, pp. 1031-1038.

(40) U.S. Department of Health and Human Services, "Toxicological Profile for Jet Fuels JP-4 and JP-7," Public Health Service, Agency for Toxic Substances and Disease Registry, June 1995.

(41) Edwards, T. and Maurice, L., "Surrogate Mixtures to Represent Complex Aviation And Rocket Fuels," *American Institute of Aeronautics and Astronautics*, AIAA-99-2217, 1999.

(42) *Handbook of Aviation Fuel Properties*, Coordinating Research Council, Inc., Atlanta, GA, Report no. 53, 1984.

(43) Dukek, W. G., "Aviation and Other Gas Turbine Fuels," In: Grayson M., ed. Kirk-Othmer Encyclopedia of Chemical Technology, 3rd ed., vol. 3, John Wiley & Sons, NY, pp. 328-351.
(44) IARC, "IARC Monographs on the Evaluation of Carcinogenic Risk of Chemical to Humans: Occupational Exposures in Petroleum Refining, Crude Oil and Major Petroleum Fuels," vol. 45, World Health Organization, International Agency for Research on Cancer, Lyon, France, vol. 45, pp. 119-158, 203-218.
(45) Mawid, M. A., Park, T. W., Sekar, B., Arana, C., and Aithal, S. M., "Development of a Detailed Chemical Kinetic Mechanism for Combustion of JP-7 Fuel," *American Institute of Aeronautics and Astronautics*, AIAA-2003-4939.
(46) Wehrmeyer, J. A., Serdar, Y., and Tecu, K. S., "Influence of Strain Rate and Fuel Dilution on Laminar Nonpremixed Hydrogen-Air Flame Structure: An Experimental Investigation," *Combustion and Flame*, vol. 107, 1996, pp. 125-140.
(47) Munson, B. R., Young, D. F., and Okiishi, T. H, *Fundamentals of Fluid Mechanics, Third Edition*, John Wiley & Sons, Inc., New York, 1998.
(48) Gutheil, E., and Williams, F., "A Numerical and Asymptotic Investigation of Structures of Hydrogen-Air Diffusion Flames at Pressures and Temperatures of High-Speed Combustion," *Twenty-Third Symposium (International) on Combustion*, The Combustion Institute, Pittsburg, 1998, pp. 513-521.
(49) Çengel, Y. A. and Boles, M. A., *Thermodynamics: An Engineering Approach, Third Edition*, McGraw-Hill Companies, Inc., USA, 1998.
(50) Chemical Propulsion Information Agency, "Fuels Section: JP-10," Unit No. 6, CPIA M6, The Johns Hopkins University, January 2003.
(51) Dickson, C. L., Woodward, P. W., "Aviation Turbine Fuels," National Institute for Petroleum and Energy Research, NIPER 149 PPS, Bartlesville, OK, 1987.
(52) Interagency Testing Committee, "Information Review: Petroleum Middle Distillate Fules," CRCS, Inc., Dynamac Corp., Rockville, MD, no. IR-470.
(53) Air Force, "Military Specification: Turbine Fuel, Low Volatility, JP-7," Report no. MIL-T-38219A, Write-Patterson Air Force Base, OH, Aerospace Medical Research Laboratory, Aerospace Division, Air Force Systems Command, 1977.
(54) Yaws, C. L., *Handbook of Transport Property Data: Viscosity, Thermal Conductivity, and Diffusion Coefficients of Liquids and Gases*, Library of Physico-Chemical Property Data, Gulf Publishing Company, 1995.
(55) Yaws, C.L., *Handbook of Viscosity, Volume 1: Organic Compounds C_1 to C_4*, Library of Physico-Chemical Property Data, Gulf Publishing Company, 1999.
(56) Brokaw, R. S., "The Lewis Number," *Second ASME Symposium on Thermophysical Properties*, 1962.
(57) Balakrishnan, G., Trees, D., and Williams, F.A., "An Experimental Investigation of Strain-Induced Extinction of Diluted Hydrogen-Air Counterflow Diffusion Flames," *Combutsion and Flame*, The Combustion Institute, vol. 98, no. 1/2, 1994, pp. 123-126.

(58) Trees, D., Brown, T.M., Seshadri, K., Smooke, M.D., Balakrishnan, G., Pitz, R.W., Giovangigli, V., and Nandula, S.P., "The Structure of Nonpremixed H_2/Air Flames," *Combustion Science and Technology*, vol. 104, 1995, pp. 427-439.

VITA

Janet Leigh Convery was born in Richmond, Virginia on July 19, 1978, and grew up in Solon, Ohio with her parents, James and Aimee, and three older siblings, Mary, Richard, and Kathy. After graduating from Solon High School in June of 1996, she began her undergraduate studies in Mechanical Engineering at Virginia Polytechnic Institute and State University in Blacksburg, Virginia. In May 2001 she graduated Cum Laude with her Bachelor of Science degree, a minor in Mathematics, and a year of Cooperative Education experience at Swales Aerospace in Beltsville, Maryland. For the following two years she worked as a civil servant for the U.S. Army at Fort Eustace, Virginia. She performed research and development of gas turbine engines in the Power Systems Division of the Aviation Applied Technology Directorate. In August of 2003, she began her Master of Science program with Virginia Tech in conjunction with NASA Langley Research Center, in the Hypersonic Air Breathing Propulsion Branch, and the National Institute of Aerospace in Hampton, Virginia. Upon completion of the program she will join the Combustion Center of Excellence at General Electric Aircraft Engines in Evendale, Ohio.